

國立交通大學

光電工程研究所

碩士論文

針對光學成像系統不同應用之
相位片之分析與設計



Design and Analysis of the Phase Plate Used in the
Applications of Optical Imaging System

研究生：詹志雲

指導教授：陳志隆 博士

中華民國九十四年六月

針對光學成像系統不同應用之相位片之分析與設計

Design and Analysis of the Phase Plate Used in
The Applications of Optical Imaging System

研究生：詹志雲
指導教授：陳志隆

Student: Chih-Yun Chan
Advisor: Jyh-Long Chern



Submitted to Institute of Electro-Optical Engineering
National Chiao Tung University
in Partial Fulfillment of the Requirements
for the Degree of
Master
in
Electro-Optical Engineering

June 2005

Hsinchu, Taiwan

中華民國九十四年六月

針對光學成像系統不同應用之相位片之分析與設計

學生: 詹志雲

指導教授: 陳志隆

國立交通大學光電工程研究所碩士班

摘要



在本論文中，我們首先提出一個環狀對稱之相位型濾波片的設計，用於緩和三階與五階球差對系統成像品質所造成之影響。接續以上的概念，我們進一步將此設計延伸至同時考量雙波長的情況下，改善系統對球差的容忍度。藉由使用所設計的濾波片，光學系統對球差的容忍度已明顯地提高，但相對而言將使調制轉換函數產生惡化。接著，我們提出一個具有四個環帶的濾波片之設計，用於使光學系統在兩個不同的波長下，能同時達到超越繞射極限的效果。最後，我們對此論文做了一個簡要的總結。

Design and Analysis of the Phase Plate Used in The Applications of Optical Imaging System

Student: Chih-Yun Chan

Advisor: Dr. Jyh-Long Chern

Institute of Electro-Optical Engineering
National Chiao Tung University

Abstract

In this thesis, we first present a radially symmetric phase-only filter to help alleviate the effects caused by the fluctuation of the third- and fifth-order spherical aberrations simultaneously. Furthermore, this idea is extended to the design of considering the system tolerance to spherical aberrations for dual wavelengths at the same time. It has been detailed that the use of the proposed phase filter indeed enhances the system tolerance to spherical aberrations, but causes a reduction in intensity and the MTF, as a tradeoff. Next, we present a method of designing a rotationally symmetric superresolving four-zone plate for dual wavelengths. The system performance of the design is shown in this thesis, with discussions in details. In the end, we draw the conclusions.

誌謝

韶光逝若水，待留無計；良景難再覓，留待追憶…

在交通大學匆匆一年半的日子裡，很高興有這難得的機會與大家相識。和大家相處的這段時間，經歷了好多好多驚奇、有趣的事，每每憶起，總也讓人不由地會心一笑，似若前刻才剛從眼前發生一般，感覺總是那麼地真實、貼近。但怎沒意料到，這匆匆不經意開始的相識，沒想到再見面時分，竟已要別離。縱然諸多不捨、心疼，亦不能如之奈何。當歌對酒醉杜康，但求此時此刻，彼此心靈依然交通。

首先要感謝陳志隆老師的諄諄教誨，並包容了我的怠惰；特別感激老師，即便在出國忙碌時分，仍透過越洋電話，關切我的論文撰寫進度，給予了寶貴的建議和提醒。還要感謝師母，常以輕鬆的談話方式，分享了許多寶貴的生活經驗。博士班的兆璽學長、淑君學姊、介任學長、以及依凱學長，感謝你們在我論文撰寫過程中，費心給予諸多的建議與協助，讓這篇碩士論文的基礎得以成型。特別感謝兆璽學長，除了學業上的指導外，更不時聆聽我發情感上的牢騷，費盡苦心引領我有更積極、樂觀的生活態度；佔去他太多私人時間，對此讓我對他的家人極為過意不去。碩士班的家佑學長、清祥學長、晟傑學長、森年學長和慧文學姊，感謝你們接納了我這碩 1.5 級的怪怪學弟。特別在口試前大家都手慌腳忙之際，仍不時表達關懷之意，心裡極其感激。碩一的同学們：忠穎，夢華，家瑜，玫君，奎佐，建成，以及燃宏大哥，謝謝你們，你們的到來，為實驗室帶來了歡樂的氣氛，包羅萬象的團購，更讓我得解嘴饞之苦。更謝謝大家，實驗室忙碌之餘，還包容了我冷笑話的疲勞轟炸，萬分對不住大家。

此外，平日有賴許多朋友給予精神上、情感上的支持，更一同在青春年華，譜寫頁頁動人的篇章。摯友博元、君杰、瑜仁，謝謝你們，即時忙得再怎麼不可開交，每年總是貼心地在我生日當天，不忘透過電話給我無限的祝福。立偉、建中、暉哥，真不好意思，常拉著你們到處去遊山玩水，現在凝望當時的照片，還真後悔當時怎沒多照幾張！青沂、宇淳、Terry、熊大、豪大、BuBu、蔡凱，還記得大家曾聚在一起，一同徹夜為中華隊加油，有時甚至瞎混到不知天之大白；那歡樂的時光，總讓人覺得過得好快。教會的孟姐、David 大哥、玉芳姐、佩玲姐、佩原、士傑等等親愛的主內弟兄姐妹，謝謝你們體恤我的軟弱，並時刻為我禱告，感謝神，讓我能認識了你們！掛一漏萬，尚有許多未提及的朋友們，在此均一併致謝。

最後要感謝爸爸、媽媽和哥哥！感謝您們長久以來全力的支持，不時給我打氣、加油，讓我能像個小頑童般，終日無憂無慮地在學術領域上盡情揮灑。在此要把完成這篇論文的喜悅，百分百地獻與我親愛的家人。

Contents

TABLE OF CONTENTS

	<u>Page</u>
1. Introduction.....	1
1.1 Background Study.....	1
1.1.1 Linear Systems Theory Applied to Optical Imaging	2
1.1.2 Coherent Imaging.....	2
1.1.3 Incoherent Imaging	3
1.2 Historical Review and Current Trends of Pupil Filters	5
1.3 Surveys of The Previous Literatures.....	7
1.3.1 Tables of Previous Literatures	7
1.3.2 A Brief Summary of the Previous Literatures.....	9
1.4 Motivation of Thesis Work	11
1.5 Organization of This Thesis	11

TABLE OF CONTENTS (CONTINUED)

	<u>Page</u>
2. Phase pupil functions for superior tolerance of spherical aberrations in large-aperture optical systems.....	13
2.1 Brief History Review	13
2.2 Basic Theory	14
2.3 Illustration and Simulation Verification.....	16
2.3.1 A phase Filter That Has Been Developed for $W_{040}=W_{020}=0$	16
2.3.2 Optimized Reduction of Spherical Aberration with Maréchal Treatment	20
2.4 Conclusions.....	27
3. Phase pupil filters employed in minimization of variation of Strehl ratio with defocus and spherical aberration for dual wavelengths	29
3.1 Basic Theory	29
3.2 Illustration and Simulation Verification.....	33
3.3 Conclusions.....	37
4. Pupil filters designed for simultaneously achieving super-resolution for two different wavelengths.....	38
4.1 Brief History Review	38
4.2 Basic Theory for Super-resolution.....	39
4.2.1 The 2 nd order expansion of the intensity distribution for small displacements of the focus position from geometrical focus.....	39
4.2.2 The 2 nd order expansion of the intensity distribution to the case in which the best image plane is not near the paraxial focus.....	42

TABLE OF CONTENTS (CONTINUED)


	<u>Page</u>
4.2.3 Fourier Optical Transformations.....	43
4.3 Structure of Hybrid Dual Focus Lens	43
4.4 Set-up of The Four-zone Pupil Filter	45
4.5 Illustration and Simulation Verification.....	49
4.5.1 Design Procedure	49
4.5.2 Simulation Verification	50
4.6 Conclusions.....	59
5 Conclusions and Future Work	60
5.1 Conclusions.....	60
5.2 Future Work	61
	
Appendix	
A. Derivation of The Pupil Phase Functions	61
A.1 Derivation of The Phase Filter That Has Been Developed for $W_{040}=W_{020}=0$	61
A.2 Derivation of The Phase Filter with Maréchal Treatment.....	63
B. More Information for 2 nd order Approximation Theory.....	64
B.1 Further Discussion to The 2 nd -order Approximation Theory	64
B.2 Modification to the Expressions of The Axial and The Transverse Gain.....	65

TABLE OF CONTENTS (CONTINUED)

	<u>Page</u>
C. MATLAB Source Codes	67
C.1 The Strehl ratio as a function of aberration coefficient W_{060}	67
C.2 Plot of the shape of the designed pupil phase function	68
C.3 Computed MTF with initial setting $W_{020}=0$ and $W_{040}=0$	69
C.4 Maximal on-axis intensity versus B_{46}	71
C.5 Plot of the Strehl ratio versus B_{26} for different aberration scaling factors f , with $B_{46} = -1.5$	72
C.6 The Strehl ratio as a function of aberration scaling factor f , with $B_{26}=0.6$ and $B_{46} = -1.5$	75
C.7 1) Relation among the transverse gain and the radius of the first zone 2) Relation among the Strehl ratio and the radius of the first zone (For CD)	78
C.8 1) Relation among the transverse gain and the radius of the first zone 2) Relation among the Strehl ratio and the radius of the first zone (For DVD)	78
C.9 The transverse intensity distributions (For CD)	80
C.10 The transverse intensity distributions (For DVD)	81
C.11 Radial intensity scans at various planes (FFT method)	82
Bibliography	83

LIST OF FIGURES

	<u>Page</u>
Fig. 1.1: Linear Systems Theory Applied To Optical Systems.....	2
Fig. 1.2: Imaging with coherent light, magnification =1.	3
Fig. 1.3: Imaging with incoherent light, magnification =1.	4
Fig. 1.4: Fraunhofer diffraction via linear system.	4
Fig. 2.1: The Strehl ratio as a function of aberration coefficient W_{060} , with zero defocus and SA3 ($W_{020}=0$ and $W_{040}=0$). The solid curve represents an ideal lens, while the dashed one corresponds to the use of the phase filter ($\beta=7\pi$; $\beta_o = 0.3*\beta$).	17
Fig. 2.2: The shape of the designed pupil phase function. (see text).....	18
Fig. 2.3: The transverse intensity distribution as a function of the aberration coefficient W_{060} (the range explored here is -2.5 to 2.5)	
(a) with clear aperture	18
(b) with the filter	19
Fig. 2.4: Computed MTF with initial setting $W_{020}=0$ and $W_{040}=0$	19
(a) Ideal lens and.....	19
(b) with the proposed phase filter, in which the solid curve: $W_{060}=0$, the dashed curve: $W_{060}=0.5\lambda$, the dotted curve: $W_{060}=\lambda$, and the dash-dot curve: $W_{060}=2\lambda$	19
Fig. 2.5: Maximal on-axis intensity versus B_{46}	22

LIST OF FIGURES (CONTINUED)

	<u>Page</u>
Fig. 2.6: Plot of the Strehl ratio versus B_{26} for different aberration scaling factors f , with $B_{46} = -1.5$.	23
(a) Ideal lens and	23
(b) with the proposed phase filter.	23
Fig. 2.7: The Strehl ratio as a function of aberration scaling factor f , with $B_{26} = 0.6$ and $B_{46} = -1.5$. The solid curve represents an ideal lens, while the dashed one corresponds to the use of the phase filter ($\beta = 5\pi$; $\beta_0 = 0.3*\beta$)	24
Fig. 2.8: The shape of the designed pupil phase function (see text).	24
Fig. 2.9: The transverse intensity distribution as a function of the aberration scaling factor f (the range explored here is 0 to 10)	
(a) with clear aperture	25
(b) with the filter	25
Fig. 2.10: Computed MTF (a) the ideal lens and (b) the proposed phase filter	26
Fig. 3.1: Fig. 3.1 Relation among 1) the intensity and 2) the enhanced factor of tolerance to the deviation of the wavelength with the use of the designed filter	34
Fig. 3.2 The Strehl ratio as a function of aberration coefficient W_{040} , with zero defocus ($W_{020}=0$). The solid curve represents an ideal lens, while the dashed one corresponds to the use of the phase filter (where $\alpha_1 = 5.6\pi$ and $\alpha_2 = 0.401*\alpha_1$)	35
(a) for the case: $A_1 = \alpha_1*(1+0.112)$ and $A_2 = \alpha_2*(1+0.112)$	35
(b) for the case: $B_1 = \alpha_1*(1-0.112)$ and $B_2 = \alpha_2*(1-0.112)$	35

LIST OF FIGURES (CONTINUED)

	<u>Page</u>
Fig. 3.3 Computed MTF with initial setting $W_{020}=0$ with the proposed phase filter (where $\alpha_1= 5.6\pi$ and $\alpha_2= 0.401*\alpha_1$), in which the solid curve: $W_{040}=0$, the dashed curve: $W_{040}=0.5\lambda$, the dotted curve: $W_{040}=\lambda$, and the dash-dot curve: $W_{040}=2\lambda$.)	36
(a) for the case: $A_1 =\alpha_1*(1+0.112)$ and $A_2=\alpha_2*(1+0.112)$	36
(b) for the case: $B_1=\alpha_1*(1-0.112)$ and $B_2=\alpha_2*(1-0.112)$	36
 Fig. 4.1: Schematics of (a) the single-ring and (b) the double-ring dual focus lens.....	 44
Fig. 4.2 Schematic of the ray trace of a hybrid lens system	45
Fig. 4.3 Radial intensity distribution of a hybrid lens system at the focal plane.....	45
Fig. 4.4: Structure of the four-zone pupil filter.....	46
Fig. 4.5: Schematics of the portions of the filter for CD	46
Fig. 4.6: Schematics of the portions of the filter for DVD	47
Fig. 4.7: 1) Relation among the transverse gain and the radius of the first zone. 2) Relation among the Strehl ratio and the radius of the first zone.....	51
(a) for the case of CD.....	51
(b) for the case of DVD	51
 Fig. 4.8: The transverse intensity distributions 1) with the clear pupil, 2) with the designed filter, for $a=0.5$ (solid curve), $a=0.57$ (dashed curve), $a=0.6$ (dotted curve).....	 52
(a) for the case of CD.....	52
(b) for the case of DVD	52

LIST OF FIGURES (CONTINUED)

	<u>Page</u>
Fig. 4.9: Relation among the displacement of focus in the axial direction and the radius of the first zone.	53
(a) for the case of CD.....	53
(b) for the case of DVD	53
Fig. 4.10: The transverse intensity distributions 1) with the clear pupil, 2) with the designed filter, for $a=0.6$	55
(a) for the case of CD.....	55
(b) for the case of DVD	55
Fig. 4.11: Radial intensity scans at various planes (the range of axial coordinates, u , explored here is -6 to 6).....	56
(a) for the case of CD.....	56
(b) for the case of DVD.....	56
Fig. 4.12: 1) Relation among the displacement and the radius of the first zone. 2) Relation among the transverse gain and the radius of the first zone. 3) Relation among the Strehl ratio and the radius of the first zone.....	57
(a) for the case of CD	57
(b) for the case of DVD	57
Fig. 4.13: The transverse intensity distributions 1) with the clear pupil, 2) with the designed filter, for radius $a=0.5$; transmittance $t_1= 0.7$	58
(a) for the case of CD.....	58
(b) for the case of DVD.	58

List of Tables

page

Table 1.1 Almanac -- Previous Publications for the Topic of Phase Pupil Filters..... 7

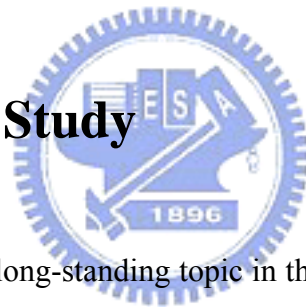
Table 1.2 Almanac -- Previous Publications for the Topic of Super-resolution 8



Chapter 1

Introduction

1.1 Background Study



Aberration theory has been a long-standing topic in the field of classical optics. The elimination of aberrations is the key issue of optical design. As we know, ray optics has been one important angle of view while dealing with this issue. However, we may sometimes find it difficult to solve the facing problem with ray optics interpretation. The wave property of light should also be carefully considered in most design cases. It can be seen that, several analysis techniques, used to examine the image quality of an optics system, are generally developed up from Fourier optics. The methods of Fourier analysis play a key role in the field of optics. Therefore, in the following pages, we will point out the key ideas of Fourier optics, briefly.

1.1.1 Linear Systems Theory Applied to Optical Imaging

Within linear systems, like most of the optical systems we considered, there exist certain fundamental relationships, which are shown in Fig. 1.1. The arrows indicate the operation required to obtain one function from another. From what we already know about diffraction and the Fourier transforms, the optical systems can be describable with linear systems theory. That is, a lens system forming an image of an object is operating within the framework of a linear system. The lens transfers the spatial frequency information of the object plane to the image plane, with some alteration. The impulse response translates each point of the object plane to a geometrically appropriate point in the image plane.

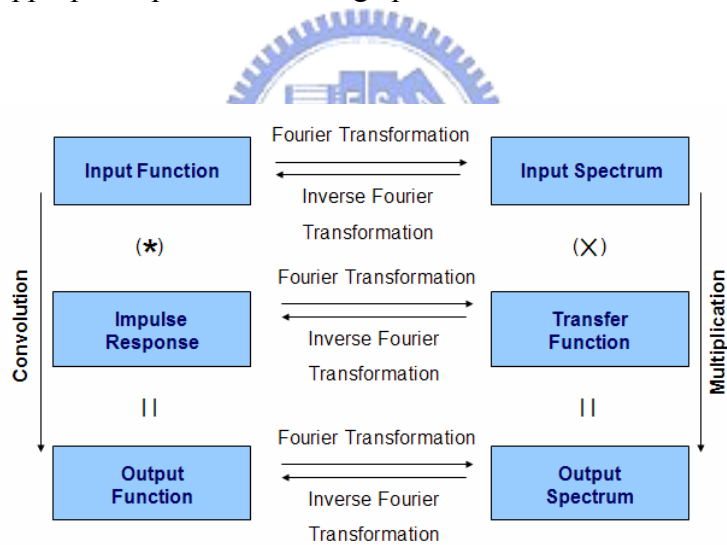


Fig. 1.1 Linear Systems Theory Applied To Optical Systems

1.1.2 Coherent Imaging

If the waves to be added are from the same source, such that there exists a fixed relationship between the phases, we say that coherence is present. Nowadays, with the advent of lasers, it becomes possible to obtain coherent light. Based on the coherent property, the linear superposition of wave amplitudes will indeed be

meaningful. If a scene is illuminated with coherent laser light and we image it with a lens, the following diagram, Fig. 1.2 is valid. The spread functions and transfer functions are mathematical constructs which describe what the optical system does to the light, transferring it from object to image.

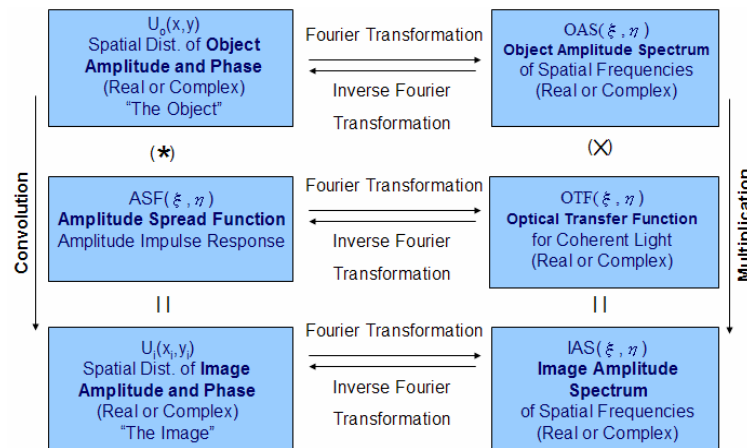


Fig. 1.2 Imaging with coherent light, $|\text{magnification}| = 1$.

1.1.3 Incoherent Imaging

If the waves are from effectively independent sources, even though monochromatic, the phase relationships of the waves converging to the image plane will not be fixed. The net effect can only be determined by statistical means like what a detector does. Thus, the only quantity describing the net effects is the average light irradiance (intensity), not amplitude, and this will require the linear superposition of irradiances (intensities). In short, the distinction we are trying to make is between amplitude and intensity. Fig. 1.3 is appropriate for incoherent illumination.

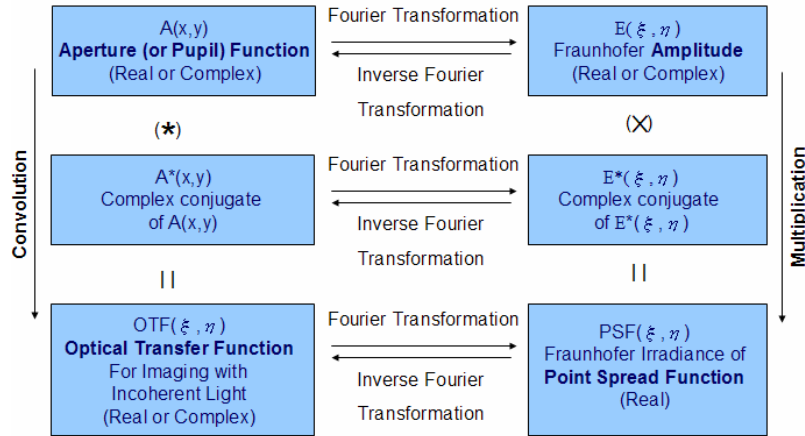
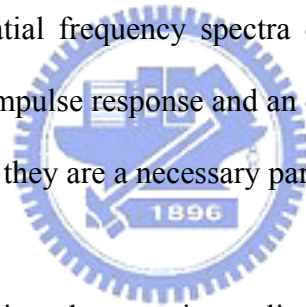


Fig. 1.3 Imaging with incoherent light, $|magnification| = 1$.

In both diagrams, Fig.1.2 and Fig.1.3, the symmetry of the Fourier transformations and inverse transformations are shown. The Fourier transform operation makes it capable of producing the spatial frequency spectra of objects and images. In the middle of both diagrams, an impulse response and an optical transfer function are also related by Fourier transforms; they are a necessary part of linear systems theory.



In Fig.1.4, the convolution theorem is applied to Fraunhofer diffraction for incoherent light. Based on this diagram, the simulation results in section 4.6 of this thesis are computed.

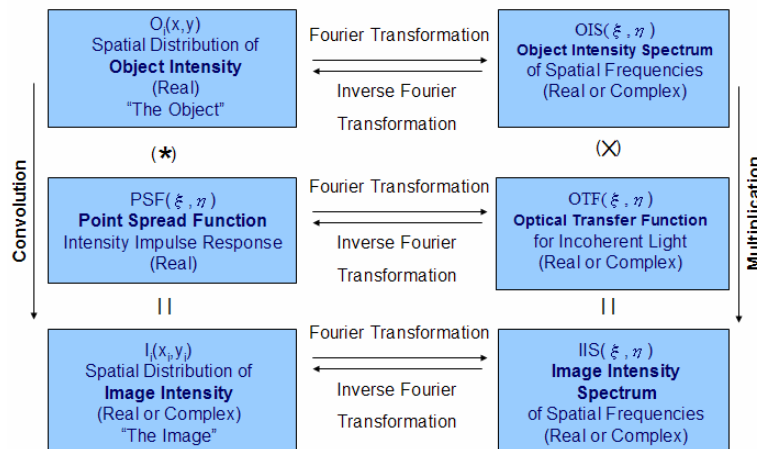


Fig.1.4 Fraunhofer diffraction via linear system.

1.2 Historical Review and Current Trends of Pupil Filters

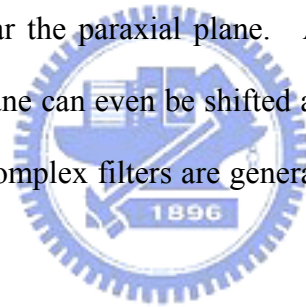
Optical systems designed to rearrange the energy distributions along three dimensional (3-D) paths near the focal spot have been analyzed extensively. As what has been reported by several authors, pupil filters can be used to modify the three dimensional response of an optical system. Different types of pupils, like amplitude-only, phase-only, or even complex-type, produce different image behavior. If these pupil filters satisfy certain symmetry condition, they can produce axial responses which are either identical or mirror reflected. It could be very useful in the filter design to produce determined 3-D optical responses if we utilize the symmetry properties of the axial and transverse response properly.

Usually, non-uniform amplitude-only filters produce effects like apodization or superresolution on the Point Spread Function (PSF) and they have been applied in several fields. For examples, apodizers have been widely used to reduce the effect of aberrations. And annular pupils have been used to achieve lateral superresolution. Other amplitude filters have also been applied in the fields like scanning imaging or microlithography.

Recently, major works have been shifted to the design of phase-only filters because these filters may have some advantages over amplitude-only filters for some critical issues, such as intensity loss issue. Different designs can be applied in

several fields like optical storage or scanning microscopy. In short, the main goal of phase filters is to control the 3-D response of the optical system to produce lateral superresolution with a specific axial response. In some cases, high depth of focus (DOF) is needed, while in other ones, axial superresolution is needed. However, the proposed forms of the phase filters could be very complicated that limit their practical application. In order to produce simple phase-filter profiles, annular phase filters or smooth varying phase functions are hence proposed.

It should be noticed that while dealing with the design case of transverse superresolution with axial superresolution, the focal behavior was studied by the transverse and axial gains for amplitude filters. These gains were later generalized for phase filters, working near the paraxial plane. And with the use of a complex pupil filter, the best image plane can even be shifted away from that without filter, so that the gain parameters for complex filters are generalized in the surroundings of the shifted focus.



1.3 Surveys of the Previous Literatures

1.3.1 Tables of Previous Literatures

Year	Publication	Provenance
1986	● Annular apodizers for low sensitivity to defocus and to spherical aberration	<i>Opt. Lett.</i>
1988	● Axial behavior of pupil-plane filters	<i>J. Opt. A- Pure Appl. Opt.</i>
1995	● Extended depth of field through wave-front coding	<i>Appl. Opt.</i>
1998	● Phase pupil functions for focal-depth enhancement derived from a Wigner distribution function,	<i>Appl. Opt.</i>
2001	● High focal depth with a pure-phase apodizer	<i>Appl. Opt.</i>
	● Electronic imaging using a logarithmic asphere	<i>Opt. Lett.</i>
2002	● Phase-shifting apodizers for increasing focal depth	<i>Appl. Opt.</i>
2003	● Combined amplitude and phase filters for increased tolerance to spherical aberration	J. Modern Opt.
	● Computational imaging with the logarithmic asphere	<i>J. Opt. A- Pure Appl. Opt.</i>
	● Extended depth of field using a logarithmic asphere	<i>J. Opt. A- Pure Appl. Opt.</i>
	● Phase pupil functions for reduction of defocus and spherical aberrations	<i>Opt. Lett.</i>
2004	● Symmetry properties with pupil phase-filters	<i>Opt. Express</i>
	● Phase plate to extend the depth of field of incoherent hybrid imaging systems	<i>Appl. Opt.</i>

Table 1.1 Almanac -- Previous Publications for the Topic of Phase Pupil Filters

Year	Publication	Provenance
1988	● Axial superresolution with phase-only pupil filters	<i>Opt. Comm.</i>
1997	● Diffractive superresolution elements	<i>J. Opt. A- Pure Appl. Opt</i>
	● Fundamental limits of optical superresolution	<i>Opt. Lett.</i>
2000	● Superresolution in far-field imaging	<i>Opt. Lett.</i>
2001	● New approach to superresolution	<i>Opt. Eng.</i>
2002	● Superresolution in far-field imaging	<i>J. Opt. A- Pure Appl. Opt</i>
	● Theories for the design of diffractive superresolution elements and limits of optical superresolution	<i>J. Opt. A- Pure Appl. Opt</i>
2003	● Design of superresolving continuous phase filters	<i>Opt. Lett.</i>
	● Design of Three-Dimensional Superresolution Filters and Limits of Axial Optical Superresolution	<i>Appl. Opt.</i>
	● Theories for the design of a hybrid refractive-diffractive superresolution lens with high numerical aperture	<i>J. Opt. A- Pure Appl. Opt</i>
	● Transverse or axial superresolution in a 4Pi-confocal microscope by phase-only filters	<i>J. Opt. A- Pure Appl. Opt</i>
2004	● Comparison of superresolution effects with annular phase and amplitude filters	<i>Appl. Opt.</i>
	● Design and comparison of amplitude-type and phase-only transverse super-resolving pupil filters	<i>Opt. Comm.</i>
	● Simple expressions for performance parameters of complex filters, with applications to super-Gaussian phase filters	<i>Opt. Lett.</i>
	● Superresolution in compensated telescopes	<i>Opt. Lett.</i>
	● Three-dimensional control of the focal light intensity distribution by analytically designed phase masks	<i>Opt. Comm.</i>
2005	● Design theories and performance limits of diffractive superresolution elements with the highest sidelobe suppressed	<i>J. Opt. A- Pure Appl. Opt</i>
	● Three-dimensional superresolution by three-zone complex pupil filters	<i>J. Opt. A- Pure Appl. Opt</i>

Table 1.2 Almanac -- Previous Publications for the Topic of Super-resolution

1.3.2 A Brief Summary of The Previous Literatures

- *For the Topic of Phase Pupil Filters:*

In 1986, J. Ojeda-Castaneta and P. Andres proposed some heuristic arguments for suggesting the use of annular apodizers with the purpose of increasing focal depth and decreasing the influence of spherical aberration. They showed that some annular apodizers can be expected to produce low sensitivity to defocus and to spherical aberration. Later on, in 1988, C. J. R. Sheppard and Z. S. Hegedus presented the relationship between the transverse and the on-axis behaviors of various pupil-plane filters. And expressions for general energy constraints associated with these filters were also derived. Then in the following years, several types of pupil filters, mainly based on amplitude modulation, were being proposed to help control the 3-D response of the optical system. But, because of the intensity loss issue, major works were soon being shifted to the design of phase-only filters. Several methods for obtaining phase-type pupil filters, providing optimization of the axial intensity distribution, and giving rise to an increase of the image focal depth, were proposed.

In 2003, Mezouari and Harvey presented a succinct way to design a phase filter with application of stationary phase approximation. By essentially developed a differential equation of wavefront error coefficients, it leads to the phase pupil function for the desired filter. And also in the same year, J. Campos, J. C. Escalera and M. J. Yzuel published their study of different pupil symmetries which would produce a predictable image behavior. They showed that different pupil-filters, satisfying certain symmetry conditions, could produce axial responses which were either identical or mirror reflected. Differences in the symmetry properties between

amplitude-only filters and phase-only filters had also been established.

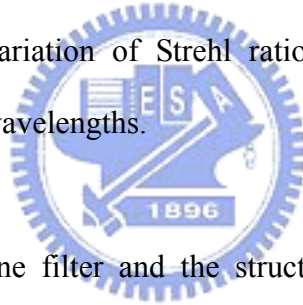
- *For the Topic of Superresolution:*

Superresolution, being able to overcome the limits of resolution, has aroused considerable interest. The study of the fundamental limits imposed on the performance of the superresolution strategy has been given by Sales and Morris in 1997. Later on, several methods have been proposed to the design of superresolving pupil filters. For instance, the diffractive superresolution elements (DSEs) with binary and multiple-phase structures were proposed by Sales and Morris; the three-zone binary phase filters were reported by Wang and Gan; and the superresolving continuous smoothly varying phase-only filters, defined to describe the effect of general complex pupil functions, were proposed by Liu, and Sun. The comparison of the performance between those proposed pupil filters has also been studied. In 2003, Ding, Li and Zhou discussed and compared the super-resolving characters of the amplitude-type and phase-type of filters. Later on, Luo and Zhou reported a comparison of the characteristics of annular amplitude and phase filters. They carefully analyzed the behavior of two-zone phase and amplitude filters.

Notice that the sidelobe effect is still one of the tough issues in the design of superresolving filters. Recently, Liu and Yan presented a theory which could be used to design a diffractive superresolution element (DSE) with the highest sidelobe suppressed.

1.4 Motivation of Thesis Work

The motivation of the first half of this thesis comes from the paper published by Mezouari and Harvey ^[10], in which they presented a way to design a phase filter by analyzing the Strehl ratio with the application of stationary phase approximation. We are interested in the design case of large-aperture optical systems, where high-order spherical aberrations have to be included. We try to derive the phase filter with improved tolerance of spherical aberrations. And also based on the concept mentioned above, we are curious if we can find out a form of pupil phase functions to minimize the variation of Strehl ratio with defocus and third-order spherical aberration for dual wavelengths.



The well-known three-zone filter and the structure of hybrid lens sparkle the motivation of the second half of this thesis. With the proposed four-zone pupil masks, we wonder if it can be practically used to improve the performance of the DVD/CD pick-up head system, through simultaneously achieving superresolution for two different wavelengths.

1.5 Organization of This Thesis

This thesis is organized as follows. In chapter 2, we first present a radially symmetric phase-only filter to help alleviate the effects caused by the fluctuation of third- and fifth-order spherical aberrations simultaneously. A performance

evaluation, including modulation transfer function, has been carried out numerically for the verification of the analytical approach. Following on, phase pupil filters employed in minimization of variation of Strehl ratio with defocus and third-order spherical aberration (SA3) for dual wavelengths are being discussed briefly. Later in chapter 3, we present a rotationally symmetric four-zone pupil masks for the goal of achieving superresolution for two different wavelengths, for which may be practically applied to the DVD/CD pick-up head system. In the final section, we draw our conclusion.



Chapter 2

Phase pupil functions for superior tolerance of spherical aberrations in large-aperture optical systems

2.1 Brief History Review



Among a variety of aberrations, defocus and spherical aberration are common and are well-recognized and manipulated optical systems along the optical axis only. Defocus and spherical aberration becomes serious in a larger aperture, even when only considering on-axis performance. The use of phase-only filters has been reported in the literature to eliminate the effect of defocus and third order Seidel aberrations, especially the spherical aberration^[1,2]. With the use of phase filters, the focal depth can be extended^[3~10]. Recently, Mezouari and Harvey presented a succinct way to design a phase filter^[10], by analyzing the Strehl ratio with the application of stationary phase approximation^[11,12]. They essentially developed a differential equation of wavefront error coefficients, efficiently leading to phase pupil function for the desired filter. Used in an imaging optical system, the designed phase

filter indeed improves the image performance, and enhances the tolerance to defocus and the third order spherical aberration^[10]. However, in many cases of optics design, the fifth order spherical aberration (SA5) is coupled with the third order spherical aberration (SA3)^[13], usually by being the negative pick-up value to each other. In other words, balancing some equal amounts of SA3 and SA5 is crucial in designing a filter for optimized reduction of spherical aberration.

In this chapter, when considering the on-axis intensity distribution of an optical system, we add one more term that corresponds to SA5 into the wave-aberration polynomial. Following the approach of Mezouari and Harvey, by requiring the on-axis intensity to be insensitive to SA5, we derive the phase filter with optimized SA reduction. For sake of self-completeness, we revisit the approach aberration variation equation with an extension to SA5. Later, numerical verification is provided. At the same time, in deducing optimized reduction of spherical aberration, we consider the classical treatment of Maréchal^[14,15] and incorporate it with the approach of Mezouari and Harvey. The result is shown in the following pages. Finally, we give our conclusion for this section.

2.2 Basic Theory

The Strehl ratio, defined as the ratio of the central intensity in the aberrated pattern to the central intensity in the unaberrated pattern, expresses the effects of the residual wavefront aberration on the image of a point source. It is given as

$$S = \left| \iint_{pupil} \exp\{i2\pi[W(\rho, \phi)]\} dA \right|^2, \quad (2.1)$$

where $W(\rho, \phi)$ is the wavefront aberration expressed as a function of the pupil in the polar coordinate system; dA is the element of are expressed as a fraction of the total area of the pupil, that is

$$dA = \rho \cdot d\rho \cdot d\phi / \iint_{pupil} \rho \cdot d\rho \cdot d\phi \quad (2.2)$$

For a circularly symmetric optical system, suffering from defocus, third- and fifth-order spherical aberration, which are W_{020} , W_{040} , and W_{060} , respectively, in terms of the wavefront aberration coefficients, the on-axis intensity is given by

$$I(W_{020}, W_{040}, W_{060}) = 4\pi^2 \left| \int_0^{\rho_0} p(\rho) \exp \left\{ 2\pi \left[W_{020} \left(\frac{\rho}{\rho_0} \right)^2 + W_{040} \left(\frac{\rho}{\rho_0} \right)^4 + W_{060} \left(\frac{\rho}{\rho_0} \right)^6 \right] \right\} \rho d\rho \right|^2 \quad (2.3)$$

where ρ is the radial coordinate over the circular pupil, and ρ_0 is the maximal radius of the pupil. Here, $p(\rho)$ is the added phase-only filter. For a radially symmetric pupil, it can be represented as

$$p(\rho) = \begin{cases} \exp[i2\pi\theta(\rho)] & 0 \leq \rho \leq \rho_0 \\ 0 & \rho \geq \rho_0 \end{cases} \quad (2.4)$$

where $\theta(\rho)$ denotes the pupil phase function. Inserting Eq.(2.4) into Eq.(2.3) with a change of variable, we will get the following term:

$$I(W_{020}, W_{040}, W_{060}) = \pi^2 \rho_0^4 \left| \int_{-\infty}^{\infty} \exp \left\{ i2\pi \left[\Phi(\xi) + W_{060} \xi^3 + \left(\frac{3}{2} W_{060} + W_{040} \right) \xi^2 + \left(\frac{3}{4} W_{060} + W_{040} + W_{020} \right) \xi + C \right] \right\} d\xi \right|^2 \quad (2.5)$$

where $\xi = (\rho / \rho_0)^2 - 1/2$, $\Phi(\xi) = \theta(\rho)$, and C is a constant phase term which will not affect the observed intensity (the integral of Eq. (2.5)) and is included for mathematical consideration and further manipulation in designing the phase filter. The pupil function is nonzero for $0 \leq \rho \leq \rho_0$, corresponding to $-1/2 \leq \xi \leq 1/2$.

The stationary phase approximation method is then applied to evaluate the value of the integral, where the stationary points are given by

$$\frac{d}{d\xi}[\Phi(\xi) + W_{060}\xi^3 + (\frac{3}{2}W_{060} + W_{040})\xi^2 + (\frac{3}{4}W_{060} + W_{040} + W_{020})\xi + C]_{\xi=\xi_s} = 0. \quad (2.6)$$

If the exponential term in Eq.(2.3) oscillates much more rapidly than the added phase filter term $p(\rho)$, the axial irradiation distribution can be approximated as:

$$I(W_{020}, W_{040}, W_{060}) \cong 2\pi^3 \rho_0^4 \left| \frac{1}{\Phi''(\xi_s) + 6W_{060}\xi_s + (3W_{060} + 2W_{040})} \right|, \quad (2.7)$$

where Φ'' represents the second derivative of Φ . If we want the on-axis irradiation distribution to be less sensitive to the variation of the fifth order spherical aberration, $W060$, then the following equation has to be established:

$$\frac{d}{dW_{060}} \left| \frac{1}{\Phi''(\xi) + 6W_{060}\xi + 3W_{060} + 2W_{040}} \right| = 0 \quad (2.8)$$

Note that Eq.(2.8) only guarantees an extreme value, which means that in order to ensure that the use of the derived form of the phase filter can really enhance the system tolerance to SA5, a further check is necessary.



2.3 Illustration and Simulation Verification

2.3.1 A Phase Filter That Has Been Developed for $W_{040}=W_{020}=0$

Here, for the purpose of illustration, we consider a phase filter that has been developed for $W_{040}=W_{020}=0$ as per Mezourari and Harvey^[10]. Next, one additional phase filter is used to tolerate SA5. In other words, the initial condition is: $W_{060} \neq 0$, $W_{040}=W_{020}=0$.

From Eq. (8), the relation between W_{060} and Φ'' can be derived as:

$$W_{060} = \frac{\Phi''}{-(6\xi + 3)} - \alpha \quad (2.9)$$

After some manipulations [see Appendix A.1], we have the phase pupil function as:

$$\theta(\rho) = \beta_0 \left(\frac{\rho}{\rho_0}\right)^6 + \beta \left(\frac{\rho}{\rho_0}\right)^6 \cdot \ln\left(\frac{\rho}{\rho_0}\right) \quad (2.10)$$

where β and β_0 provide two degrees of freedom.

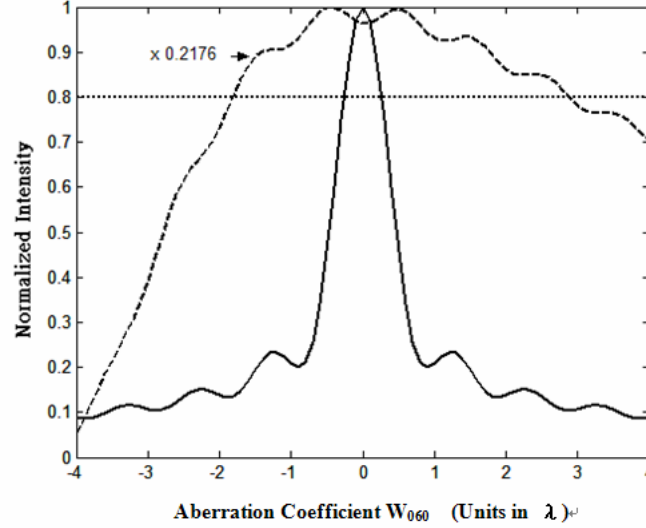


Fig. 2.1: The Strehl ratio as a function of aberration coefficient W_{060} , with zero defocus and SA3 ($W_{020}=0$ and $W_{040}=0$). The solid curve represents an ideal lens, while the dashed one corresponds to the use of the phase filter ($\beta=7\pi$; $\beta_0 = 0.3*\beta$)

The performance of the phase filter of Eq. (2.10) is shown in Fig. 2.1. As shown in Fig.2.1, with the use of the derived phase filter ($\beta = 7\pi$; $\beta_0 = 0.3*\beta$), the system has a higher tolerance to SA5. The boundary of tolerance can be judged based on Rayleigh's criterion, i.e., the normalized intensity of 0.8 is the limit for fine-correction imaging. In other words, the limit for low aberration imaging against W_{060} ranges between -1.8 and 2.8, while it ranges between -0.25 and 0.25 for an "ideal" lens, which is nearly approaching the case of diffraction-limited condition. That is, the tolerance to SA5 is improved by a factor of nine. The shape of phase pupil function is shown in Fig. 2.2 for reference. Notice that the calculated phase is

extended to a range from $-\pi$ to π .

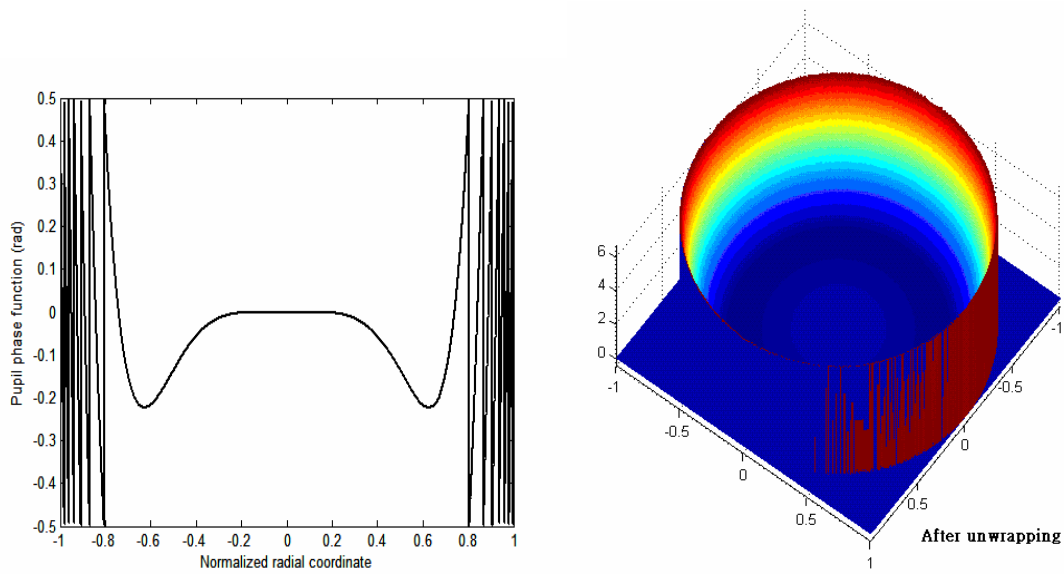
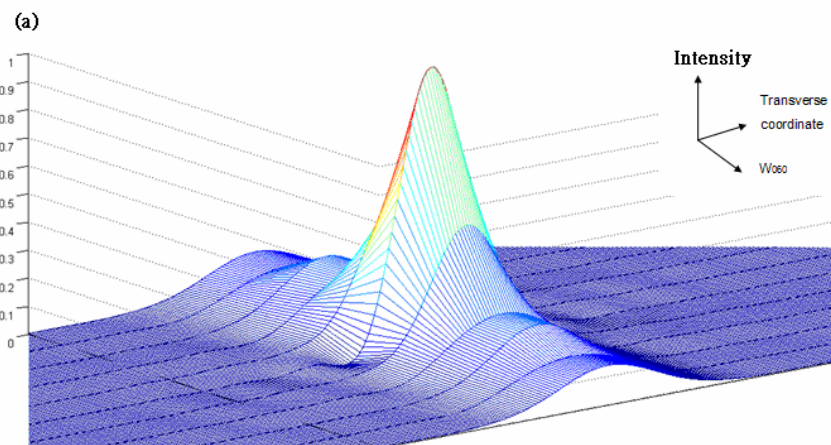


Fig. 2.2 The shape of the designed pupil phase function. (see text)

In Fig. 2.3, a plot of the transverse intensity distribution as a function of aberration coefficient W_{060} is shown. It can be seen that, with the use of the designed phase filter, the transverse intensity distribution also becomes insensitive to the variation of the residual 5th order SA, though there is a reduction in intensity because of an increase of size of the point-spread function (PSF).



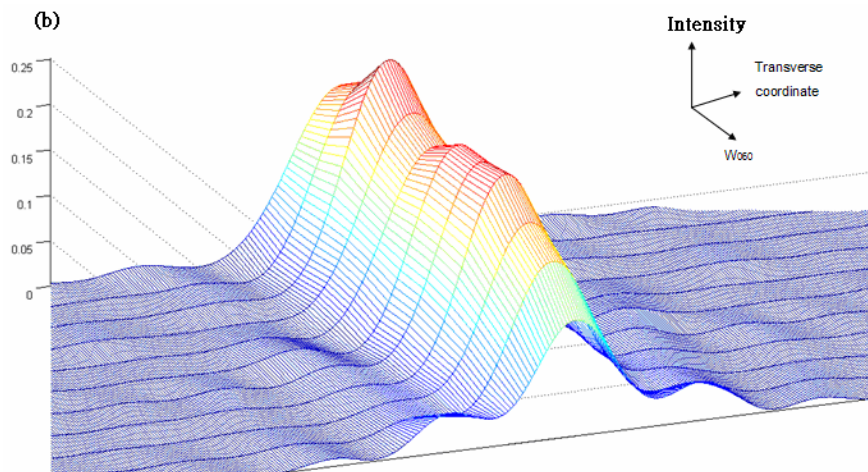


Fig. 2.3 The transverse intensity distribution as a function of aberration coefficient W_{060} , (the range explored here is -2.5 to 2.5) (a) with clear aperture (b) with the filter

To illustrate more clearly, let us take a look at the computed modulation transfer function (MTF) at different SA5s. As shown in Fig. 2.4, the MTF of an ideal circular lens is quite sensitive to the variation of the residual 5th order SA.

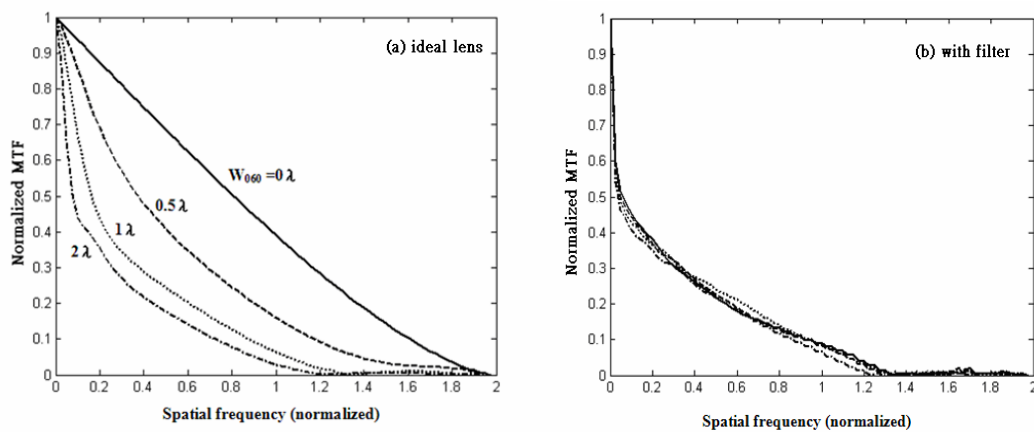


Fig. 2.4: Computed MTF with initial setting $W_{020}=0$ and $W_{040}=0$. (a) Ideal lens and (b) with the proposed phase filter, in which the solid curve: $W_{060}=0$, the dashed curve: $W_{060}=0.5\lambda$, the dotted curve: $W_{060}=\lambda$, and the dash-dot curve: $W_{060}=2\lambda$.

The MTF drops rapidly as the value of the 5th order SA increases, which implies that the image quality is badly damaged in the case of fine resolution with a higher spatial frequency. With the use of the phase filter, the MTF becomes less sensitive to the variation of SA5 and hence stabilizes the final image quality, although of course it causes a reduction in the MTF.

It must be noted that there is also a reduction of 40% in the effective cut-off spatial frequency in the case of an ideal lens. These reductions are a baseline in using the filter for practical applications of imaging optics. For instance, in some metrology applications, certain amounts of contrast (35%) and image resolution (30lp/mm) are required for accurate image edge detection. When applying the phase filter to the lens system, one should first be careful about the baselines. Although the use of phase filter drops down the MTFs than those of an ideal lens, the MTFs become much less sensitive to the aberration and contain no zeros. The zero-free of MTFs makes it possible for digital restoration of the recorded image, which permits an almost diffraction-limited PSF to be retrieved.

2.3.2 Optimized Reduction of Spherical Aberration with Maréchal Treatment

In this section, we will discuss the development of a phase-only filter with the initial condition of a fixed ratio of W_{040}/W_{060} . It is known that when the axial irradiation distribution I is greater than 0.8, it may be approximated as

$$I = |1 - (\frac{2\pi^2}{\lambda^2})E|^2 \quad (2.11)$$

where

$$E = \iint_{pupil} W^2(r, \phi) dA - [\iint_{pupil} W(r, \phi) dA]^2 \quad (2.12)$$

is the variance of $W(r, \phi)$ over the pupil of the optical system [14,15]. Based on Maréchal's treatment of the tolerance theory, the value of variance E may serve as a useful criterion in designing a high-quality optical system [14,15]. Cross-referencing to Eq. (2.1), W is the residual wave-front aberration on the exit pupil. In this section, the main aberrations of concern are defocus, SA3, and SA5, and as such the wave-aberration polynomial W will be expressed as:

$$W = f(B_{26}\rho^2 + B_{46}\rho^4 + 1.0\rho^6), \quad (2.13)$$

where B_{26} and B_{46} represent the ratios of W_{020}/W_{060} and W_{040}/W_{060} respectively, and f is the aberration scaling factor, which is proportional to the value of W_{060} in Eq. (2.2). The use of the aberration scaling factor f permits the argument of the exponential function in Eq. (2.1) to be varied. This helps us to analyze the influence on the Strehl ratio of aberrations of different magnitudes. Maréchal has shown that, for spherical aberration the best form of correction (with $\partial E / \partial W_{040} = 0$) is determined by the condition $W_{040}/W_{060} = -1.5$ [16]. First, as a simple illustration, the scaling factor f is taken to be 1. Then we take a close look at the variation of the maximal value of the on-axis intensity by varying the value of B_{46} . As shown in Fig. 2.5, the maximum occurs when the value of B_{46} is equal to -1.5, which corresponds exactly to the statement of Maréchal.

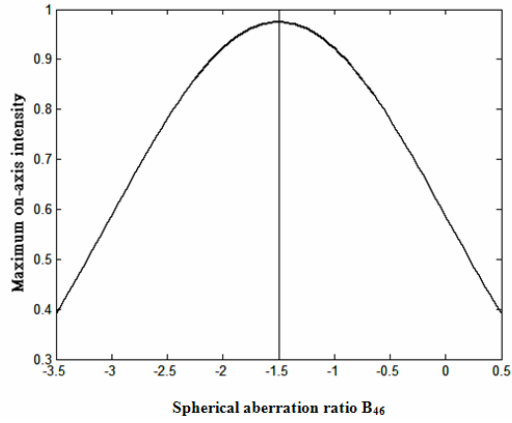


Fig. 2.5 Maximal on-axis intensity versus B_{46}

In quite a similar way shown in section 2.3.1, we derive the pupil phase function for the case that B_{46} is fixed to be -1.5. From Eq. (2.8), the relation between W_{060} and Φ'' can be derived as

$$W_{60} = \frac{\Phi''}{-6\xi} - \alpha \quad (2.14)$$

After some manipulations [see Appendix A.2], the pupil phase function is expressed as the following form:

$$\theta(\rho) = \beta_0 \left(\frac{\rho}{\rho_0}\right)^6 + \beta \left(\frac{\rho}{\rho_0}\right)^6 \cdot \ln\left(\frac{\rho}{\rho_0}\right) \quad (2.15)$$

Now, we fix the value of B_{46} to be -1.5 and vary the value of the aberration scaling factor f , so that f is from 1 to 6. With a suitable range of B_{26} values, the variations of the Strehl ratios are observed.

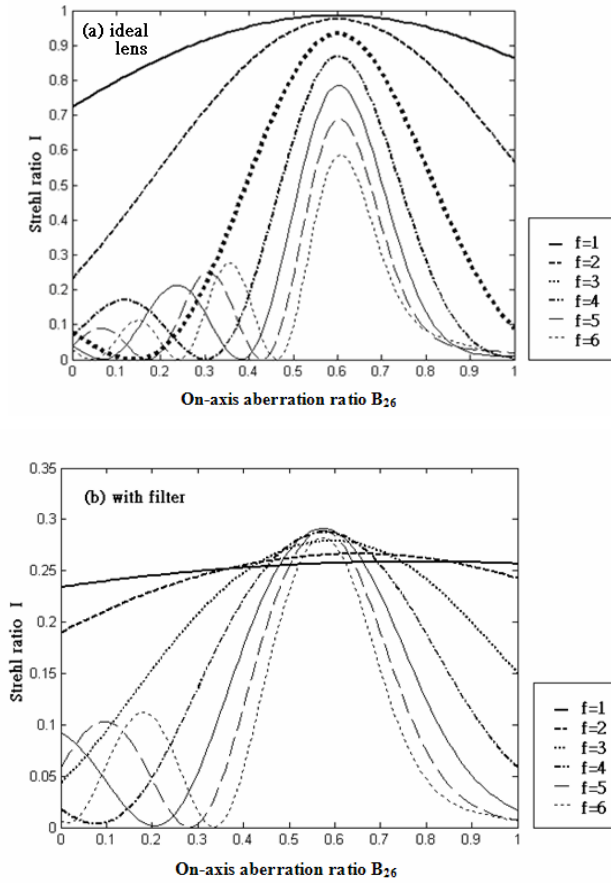


Fig. 2.6 Plot of the Strehl ratio versus B_{26} for different aberration scaling factors f , with $B_{46} = -1.5$. (a) Ideal lens and (b) with the proposed phase filter.

The computed Strehl ratios I vs B_{26} curves are shown in Fig. 2.6. For an ideal lens, the maximum value of the Strehl ratio, occurs around the value of $B_{26} = 0.6$ for each curve. As the value of the aberration scaling factor increases, the maximum value of the Strehl ratio drops rapidly. With the application of the phase filter, where $\beta = 5\pi$; $\beta_o = 0.3*\beta$, the Strehl ratio of the optical system becomes much more “condensed” at $B_{26} = 0.6$, although it causes a reduction in magnitude. Furthermore, as shown in Fig. 2.7, with the use of the filter, even if the value of the scaling factor f becomes ten times larger, the normalized on-axis intensity still remains at 75% of the maximum value, while it drops to only 20% of the maximum value in the case of an ideal lens. Therefore, with the application of the phase filter, the optical system

becomes less sensitive to the variation of the 5th order SA. The shape of phase pupil function is shown in Fig. 2.8 for reference.

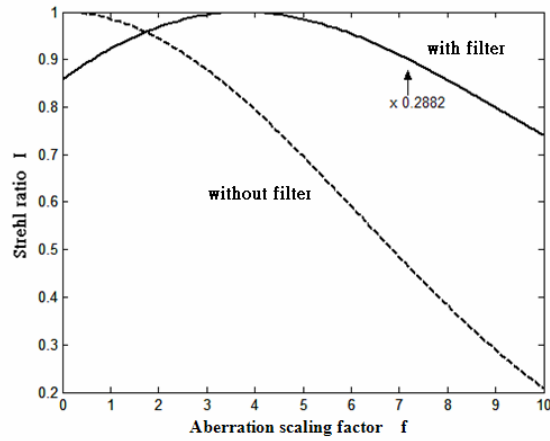


Fig. 2.7 The Strehl ratio as a function of aberration scaling factor f , with $B_{26} = 0.6$ and $B_{46} = -1.5$. The solid curve represents an ideal lens, while the dashed one corresponds to the use of the phase filter ($\beta = 5\pi$; $\beta_0 = 0.3 \cdot \beta$)

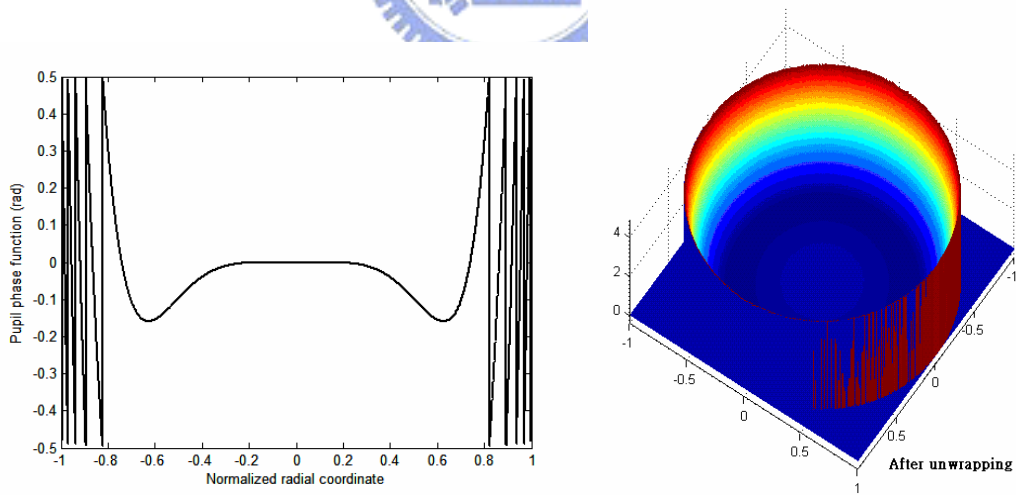


Fig. 2.8 The shape of the designed pupil phase function (see text).

Let us now shift our focus to the issue of trade-off. The transverse intensity distribution as a function of the aberration scaling factor f is shown in fig. 2.9. When the designed phase filter is applied, the transverse intensity distribution becomes insensitive to the variation of the scaling factor f . However, as a trade-off, the magnitude of the on-axis intensity has dropped to about one-third of the original one with a clear aperture.

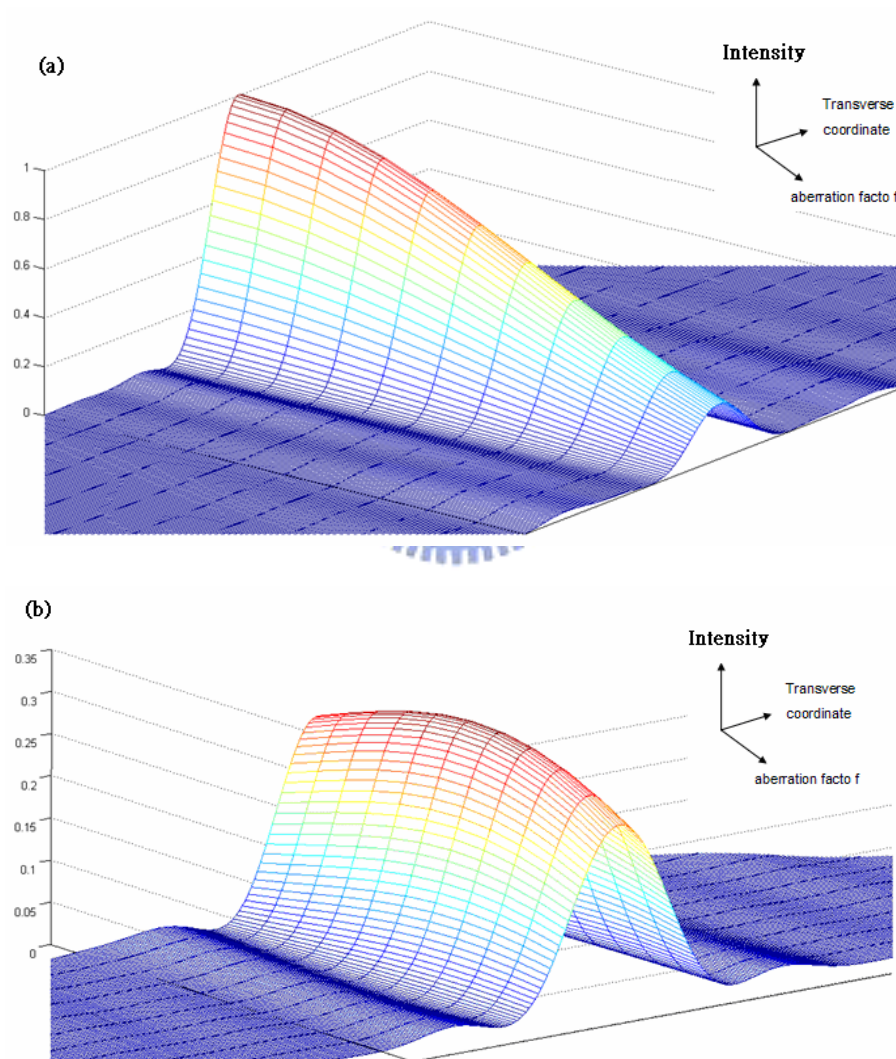


Fig. 2.9 The transverse intensity distribution as a function of the aberration scaling factor f (the range explored here is 0 to 10) (a) with clear aperture (b) with the filter

Next, we look at the MTF performance for different values of the scaling factor, namely $f = 0, 2, 4, 6,$ and 8 , where $B_{26} = 0.6,$ $B_{46} = -1.5$ are fixed correspondingly. As shown in Fig. 2.10, the MTF of an ideal circular lens fluctuates greatly with the variation of the scaling factor. When the phase filter is applied, the MTF becomes much more insensitive to the variation of the scaling factor, although it causes a reduction in the MTF, and the effective cut-off frequency now becomes 70% of the ideal lens case.

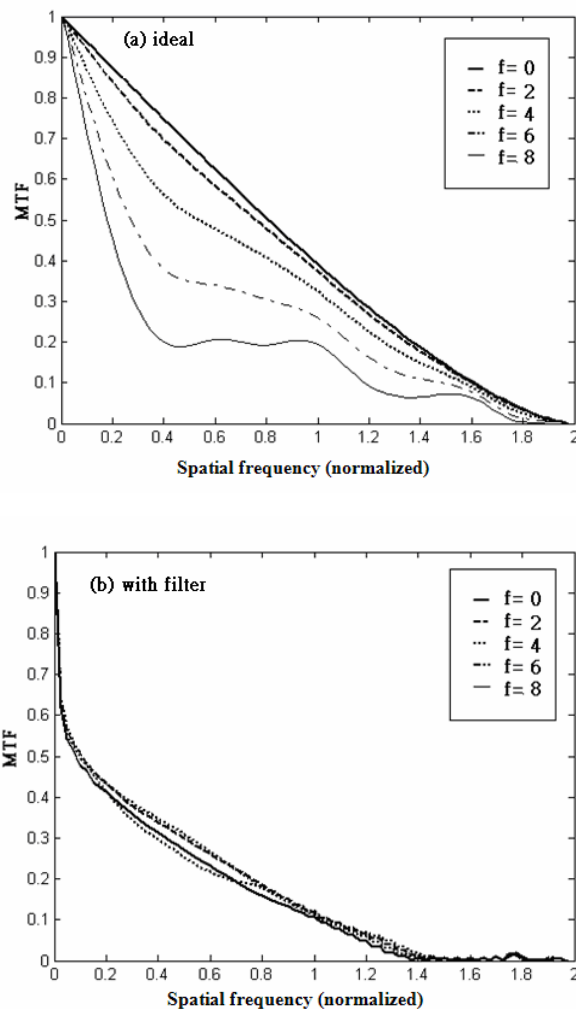


Fig. 2.10 Computed MTF with (a) the ideal lens and (b) the proposed phase filter.

2.4 Conclusions

In conclusion, we derived a radially symmetric phase-only filter that enhances the system tolerance to an SA5 by using the method of stationary phase approximation similar to the approach of Mezouari and Harvey. Two different implementations have been provided. The proposed approaches of extension and its deduced phase filters will be especially useful in the case when the imaging optical system has a large size of aperture. Which one is better is, of course, dependent on the inherent characteristics of optical systems over the leading and different orders of aberration. Inclusion of Maréchal treatment in the approach of Mezouari and Harveys is an efficient method to deduce a phase filter with superior tolerance in defocus and spherical aberration as well as better system performance of imaging quality.

The critical issue of trade-off is worthwhile to be readdressed; it has been detailed that the use of the proposed phase filter causes a reduction in intensity and the MTF. These reductions form the baselines in practical applications of the use of phase filter. Optimization has to be reconsidered in developing the filters to meet the performance requirements and/or system specifications. It is worth noting that the pupil phase function in a logarithmic form is in fact a particular solution of the developed differential equations. That is to say, this solution form has been obtained by assigning the added constants to some particular values. This is the freedom and the advantage of the approach of Mezouari and Harvey in deducing an optimized solution of phase filter. In this section, in contrast, it is the capability of “superior tolerance” to be addressed. In other words, one of main goals of this section is to

investigate how “superior” can be established in tolerance based on the approach of Mezouari and Harvey (an approach with solving the different equations of aberration coefficients). Finally, as a comment, it is a simple and straightforward matter to determine the extension to a higher order spherical aberration (say, the seventh order spherical aberration, SA7), which could be more critical in the systems with larger aperture.



Chapter 3

Phase pupil filters employed in minimization of variation of Strehl ratio with defocus and spherical aberration for dual wavelengths



3.1 Basic theory

For the collimated light passing through an objective lens and a phase-shifting apodizer and then converging through onto an optical disk, the normalized amplitude distribution in the image side can be defined as ^[1-3]:

$$G(\rho, u) = \int_0^{r_{\max}} p(r) \cdot J_0(\rho r) \cdot \exp[-i \frac{u}{2} r^2] \cdot r dr \quad (3.1)$$

ρ and u are the simplified radial and axial coordinates, respectively, on the image side:

$$\rho = \frac{2\pi}{\lambda} (NA) \cdot R \quad u = \frac{2\pi}{\lambda} (NA)^2 \cdot Z \quad (3.2)$$

where R and Z are the radial and axial coordinates on the image side. NA is the numerical aperture of the objective lens. Here, $P(r)$ represents the generalized pupil function, which for a radially symmetric pupil can be represented as

$$p(r) = \begin{cases} \exp[i2\pi\theta(r)] & 0 \leq r \leq r_{\max} \\ 0 & r \geq r_{\max} \end{cases} \quad (3.3)$$

Therefore, the on-axis amplitude distribution function in the focal region can be expressed as:

$$G(\rho, u) = \int_0^{r_{\max}} \exp\left\{i \cdot \frac{2\pi}{\lambda} [n \cdot \theta(r) - (NA)^2 \cdot (z - f) \cdot r^2]\right\} \cdot r dr \quad (3.4)$$

Now, if we mainly consider about the effect of defocus and third order spherical aberration (SA3) to the on-axis performance of an optical system, the on-axis intensity distribution is then given by:

$$I(W_{20}, W_{40}) = 4\pi^2 \left| \int_0^{r_{\max}} \exp\left\{i \frac{2\pi}{\lambda} [n \cdot \theta(r) - NA^2 \Delta z \cdot r^2 + W_{020} r^2 + W_{040} r^4]\right\} r dr \right|^2 \quad (3.5)$$

As the frequency of the incident collimated light varies, the resulting magnitude of defocus (or SA3) will change. Here comes an important issue that we have to find out a relationship between those aberration terms and the frequencies. If the amount of variation of the frequency is small, it is reasonable to state that there still remains a linear relation between the aberration terms and the frequency.

Note that the primary aberration terms, up to fourth order in pupil and object or image coordinates, can be expressed as ^[4-8]:

$$W(r, \theta; h') = a_{ss} r^4 + a_{cs} h' r^3 \cos \theta + a_{as} h'^2 r^2 \cos^2 \theta + a_{ds} h'^2 r^2 + a_{is} h'^3 r \cos \theta \quad (3.6)$$

where those five terms refer to spherical aberration, coma, astigmatism, Petzval curvature and distortion. To evaluate the on-axis performance of an optical system, we mainly pay our attention to the first term, SA3. And for a thin lens system, the coefficient a_{ss} , is given by:

$$a_{ss} = -\frac{1}{32n(n-1)f^3} \left[\frac{n^3}{n-1} + (3n+2)(n-1)p^2 + \frac{n+2}{n-1}q^2 + 4(n+1)pq \right] \quad (3.7)$$

where p and q are called the position and shape factors, respectively.

$$p = (2f / S) - 1 = 1 - 2f / S' \quad (3.8)$$

$$q = (R_2 + R_1) / (R_2 - R_1) \quad (3.9)$$

S and S' refer to the object distance and the image distance, and R₁ and R₂ are the radii of curvature of the two surfaces of the lens.

If the position factor is given, the value of the shape factor which minimizes the spherical aberration is given by the condition:

$$\frac{\partial a_{ss}}{\partial q} = 0 \quad (3.10)$$

Thus, we obtain

$$q_{\min} = -2p \frac{n^2 - 2}{n + 2} \quad (3.11)$$

For the case that an object is at infinity and the image is at the focal plane of the lens, the value of the position factor p is set to be 1. Substituting the above Eq. 3.11 into Eq.3.7, hence the corresponding minimum spherical aberration is obtained:

$$a_{ss \min} = \frac{1}{32f^3} \left[\left(\frac{n}{n-1} \right)^2 - \frac{n}{n+2} p^2 \right] \quad (3.12)$$

Thus, the wave-front aberrations for two different incident light frequencies can be expressed as:

$$W_{\lambda_1} = n_1 \theta(r) + a_1 W_{020} r^2 + a_2 (W_{040 \min}^{\lambda_1} + W_{040}) r^4 \quad (3.13-1)$$

$$W_{\lambda_2} = n_2 \theta(r) + b_1 W_{020} r^2 + b_2 (W_{040 \min}^{\lambda_2} + W_{040}) r^4 \quad (3.13-2)$$

Where

$$W_{040 \min}^{\lambda_1} = \frac{1}{f_2^3} \left[\left(\frac{n_1}{n_1 - 1} \right)^2 - \frac{n_1}{n_1 + 2} \right] \quad (3.14-1)$$

$$W_{040 \min}^{\lambda_2} = \frac{1}{f_2^3} \left[\left(\frac{n_2}{n_2 - 1} \right)^2 - \frac{n_2}{n_2 + 2} \right] \quad (3.14-2)$$

With a change of variable, $\xi = r^2 - 1/2$, we get:

$$W_{\lambda_1} = n_1 \Phi(\xi) + a_2 (W_{040} + W_{040\min}^{\lambda_1}) \xi^2 + (a_1 W_{020} + a_2 (W_{040} + W_{040\min}^{\lambda_1})) \xi \quad (3.15-1)$$

$$W_{\lambda_2} = n_2 \Phi(\xi) + b_2 (W_{040} + W_{040\min}^{\lambda_2}) \xi^2 + (b_1 W_{020} + b_2 (W_{040} + W_{040\min}^{\lambda_2})) \xi \quad (3.15-2)$$

By employing the stationary phase approximation, the axial irradiation distribution is given by:

$$I_1(W_{20}, W_{40}) \cong 2\pi^3 \rho_0^4 \left| \frac{1}{2a_2 W_{040} + \Phi''(\xi_s)} \right| \quad (3.16-1)$$

$$I_2(W_{20}, W_{40}) \cong 2\pi^3 \rho_0^4 \left| \frac{1}{2b_2 W_{040} + \Phi''(\xi_s)} \right| \quad (3.16-2)$$

Notice that the stationary points for both frequencies are given by:

$$\frac{d}{d\xi} [n_1 \Phi(\xi) + a_2 W_{040} \xi^2 + (a_2 W_{40} + a_1 W_{20}) \xi]_{\xi=\xi_s} = 0 \quad (3.17-1)$$

$$\frac{d}{d\xi} [n_2 \Phi(\xi) + b_2 W_{040} \xi^2 + (b_2 W_{40} + b_1 W_{20}) \xi]_{\xi=\xi_s} = 0 \quad (3.17-2)$$

If the added phase filter is used to enhance the system tolerance to SA3 for both wavelengths, the following equations must be satisfied simultaneously:

$$\left\{ \begin{array}{l} \frac{d}{d\xi} [n_1 \Phi(\xi) + a_2 W_{040} \xi^2 + (a_2 W_{40} + a_1 W_{20}) \xi]_{\xi=\xi_s} = 0 \\ \frac{d}{dW_{40}} \left| \frac{1}{2a_2 W_{40} + \Phi''(\xi_s)} \right| = 0 \end{array} \right. \quad (3.18-1)$$

$$\left\{ \begin{array}{l} \frac{d}{d\xi} [n_2 \Phi(\xi) + b_2 W_{040} \xi^2 + (b_2 W_{40} + b_1 W_{20}) \xi]_{\xi=\xi_s} = 0 \\ \frac{d}{dW_{40}} \left| \frac{1}{2b_2 W_{40} + \Phi''(\xi_s)} \right| = 0 \end{array} \right. \quad (3.18-2)$$

Then the resulting pupil phase functions that control SA3 when the optical system is at the best focal plane will be written as:

$$\theta_{\lambda_1}(r) = A_2 r^4 + A_1 r^4 \log(r) \quad (3.19-1)$$

$$\theta_{\lambda_2}(r) = B_2 r^4 + B_1 r^4 \log(r) \quad (3.19-2)$$

Similarly, the independence of the axial irradiation distribution on defocus aberration leads to the following equations:

$$\left\{ \begin{array}{l} \frac{d}{d\xi} [n_1 \Phi(\xi) + a_2 W_{040} \xi^2 + (a_2 W_{40} + a_1 W_{20}) \xi]_{\xi=\xi_s} = 0 \\ \frac{d}{dW_{20}} \left| \frac{1}{2a_2 W_{40} + \Phi''(\xi_s)} \right| = 0 \end{array} \right. \quad (3.20-1)$$

$$\left\{ \begin{array}{l} \frac{d}{d\xi} [n_2 \Phi(\xi) + b_2 W_{040} \xi^2 + (b_2 W_{40} + b_1 W_{20}) \xi]_{\xi=\xi_s} = 0 \\ \frac{d}{dW_{20}} \left| \frac{1}{2b_2 W_{40} + \Phi''(\xi_s)} \right| = 0 \end{array} \right. \quad (3.20-2)$$

Then the resulting phase functions that reduce the defocus error when SA3 is negligible yield:

$$\theta_{\lambda_1}(r) = \alpha(r^2 - 1/2)^2 \quad (3.21-1)$$

$$\theta_{\lambda_2}(r) = \beta(r^2 - 1/2)^2 \quad (3.21-2)$$

3.2 Illustration and Simulation Verification

A DVD/CD optical pick-up head system, containing 635 and 785 nm laser diodes, is taken as an example here. Now, in order to lower down the sensitivity of the on-axis intensity of this optics system to SA3, the circular symmetric logarithmic phase filter, described in Eq.3.19, is employed. We first consider about the system performance for the wavelength which is equal to the average value of the two wavelengths. How the parameters of the pupil function are determined depends on the system requirement of the magnitude of on-axis intensity and the range of

tolerance. For instance, if we want to enhance the tolerance to SA3 for at least five times and still keeps the magnitude of the on-axis intensity at least one-tenth of the original value, we may find it a good option to set the parameters $\alpha_1 = 5.6\pi$ and $\alpha_2 = 0.401 \cdot \alpha_1$. Then we pay attention to the variation of the intensity and the tolerance to the deviation of the wavelength, as shown in Fig. 3.1. It can be seen that the corresponding changes of those terms to the deviation of the wavelength are still under control.

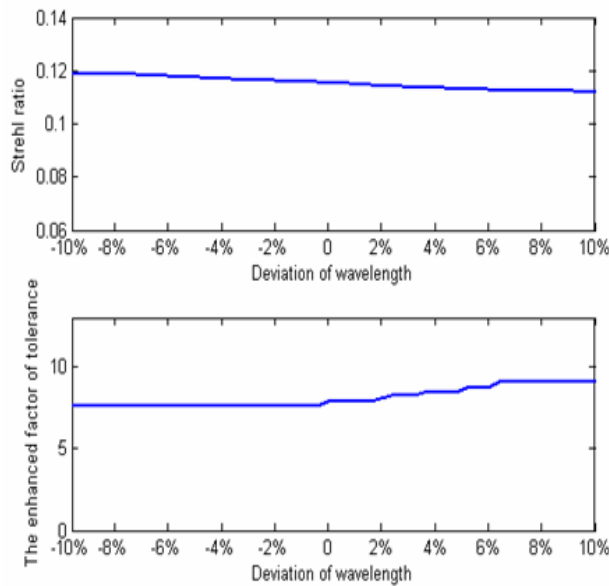


Fig. 3.1 Relation among 1) the intensity and 2) the enhanced factor of tolerance to the deviation of the wavelength with the use of the designed filter

By setting $A_1 = \alpha_1 \cdot (1 + 0.112)$ and $A_2 = \alpha_2 \cdot (1 + 0.112)$, the system tolerance to SA3 for DVD is enhanced for about seven times, as shown in Fig.3.1 (a). Meanwhile, the corresponding values of B_1 and B_2 are also determined, where $B_1 = \alpha_1 \cdot (1 - 0.112)$ and $B_2 = \alpha_2 \cdot (1 - 0.112)$, and the tolerance to SA3 for CD is improved by a factor of 6, as shown in Fig.3.2 (b). However, it should be noticed that the application of the phase filter will shift away the position of the central peak in both cases.

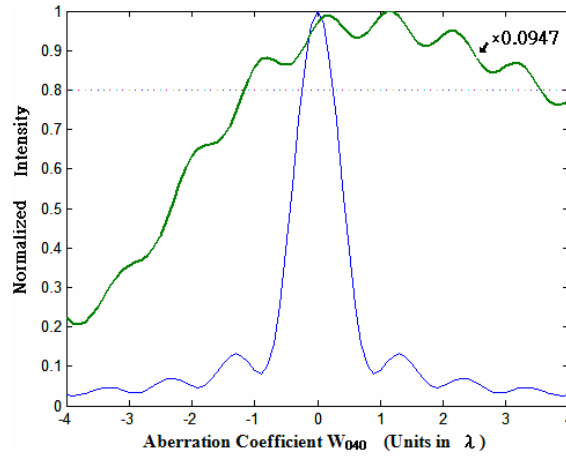


Fig. 3.1 (a)

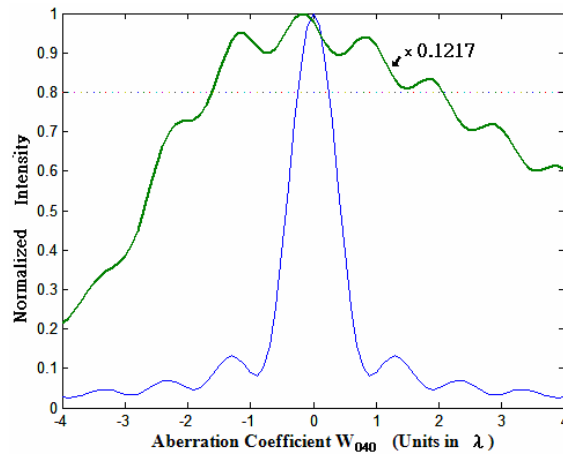


Fig. 3.2 The Strehl ratio as a function of aberration coefficient W_{040} , with zero defocus ($W_{020}=0$). The solid curve represents an ideal lens, while the dashed one corresponds to the use of the phase filter (where $\alpha_1=5.6\pi$ and $\alpha_2=0.401*\alpha_1$)

(a) for the case: $A_1=\alpha_1*(1+0.112)$ and $A_2=\alpha_2*(1+0.112)$

(b) for the case: $B_1=\alpha_1*(1-0.112)$ and $B_2=\alpha_2*(1-0.112)$

A comparison between the computed modulation transfer function (MTF) for different values of SA3 for these two wavelengths is displayed in Fig. 3.3. Originally, the MTF is sensitive to the variation of the amount of additional SA3. When the designed logarithmic phase filter is used, the MTF becomes less sensitive to

SA3 in both cases. However, there is a reduction of the effective cut-off frequency of about 45%, and a reduction in the signal-to-noise ratio.

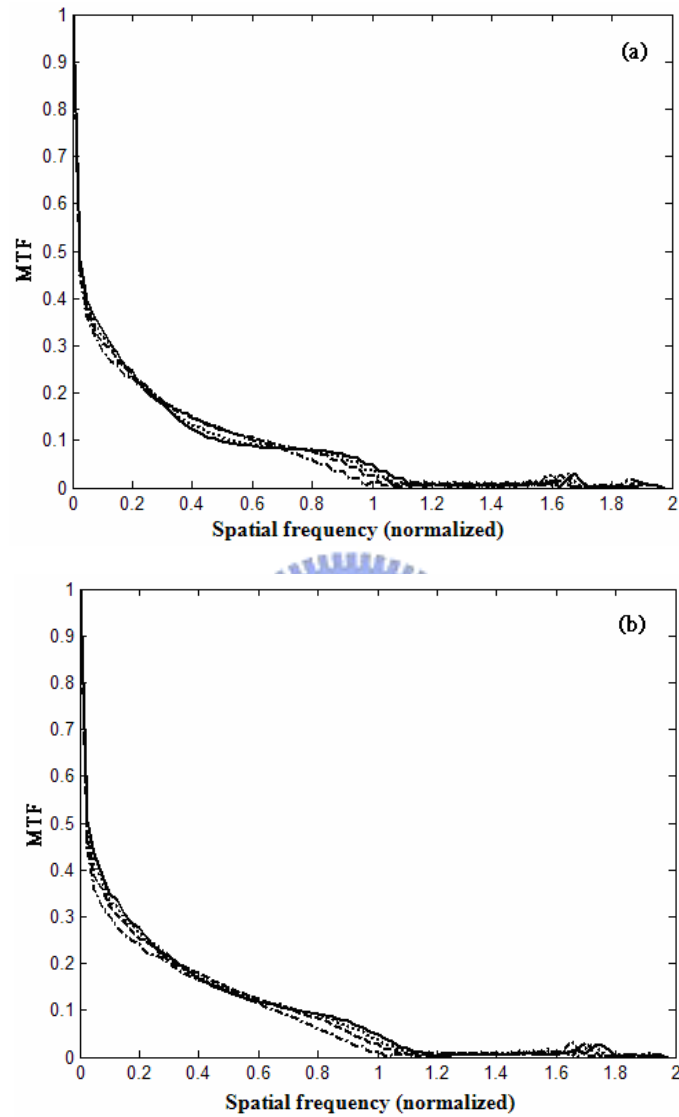


Fig. 3.3 Computed MTF with initial setting $W_{020}=0$ with the proposed phase filter (where $\alpha_1= 5.6\pi$ and $\alpha_2= 0.401*\alpha_1$), in which the solid curve: $W_{040}=0$, the dashed curve: $W_{040}=0.5\lambda$, the dotted curve: $W_{040}=\lambda$, and the dash-dot curve: $W_{040}=2\lambda$.)

(a) for the case: $A_1 =\alpha_1*(1+0.112)$ and $A_2=\alpha_2*(1+0.112)$

(b) for the case: $B_1=\alpha_1*(1-0.112)$ and $B_2=\alpha_2*(1-0.112)$,

3.3 Conclusions

In this chapter, we present a way to implement the minimization of variation of Strehl ratio with defocus and spherical aberration for dual wavelengths. By using the proposed phase pupil filters, we can see that the system tolerance to SA3 is, indeed, enhanced. However, as a trade-off, the use of the phase filters will inevitably drop down the central peak of the intensity and also the effective cut-off frequency, which leads to worsen the image quality. It should be noticed that, we make some simplification and put some constraints in the deduction of the pupil function, which will also limit the use of the designed phase filters.



Chapter 4

Pupil filters designed for simultaneously achieving super-resolution for two different wavelengths

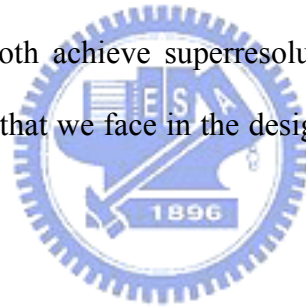
4.1 Brief History Review



Superresolution was first being discussed by Toraldo di Francia in 1952 ^[1]. Being able to overcome the limits of resolution imposed by diffraction in optical systems, this idea has aroused considerable interest, especially in the fields of optical storage and optical microscopy ^[2,3]. One can enhance the storage capability of a single compact disk by reducing the size of the focusing laser spot. Thereby, lots of methods have been proposed to designing superresolving pupil filters. At first, these filters were based on amplitude (variable-transmittance) pupils ^[4-7]. Later on, attention has been shifted to develop pure-phase filters in order to overcome some drawbacks of amplitude filters: for instance, intensity loss issue ^[8-12]. Many phase profiles that achieve transverse superresolution are based on annular designs, such as the diffractive superresolution elements (DSEs) proposed by Sales and Morris ^[2], and

the three-zone binary phase filters reported by Wang ^[13,14]. For the design of continuous superresolving phase-only profiles, the global/local united search algorithm (GLUSA) is generally used ^[15]. However, it requires extremely complex phase masks to achieve the wanted performance. In order to conquer that difficulty, superresolving continuous smoothly varying phase-only filters, obtained by using a series of figures of merit which are properly defined to describe the effect of general complex pupil functions, were proposed ^[16]. The advantages of these kinds of filters are that they don't produce energy absorption and they are easy to build with a phase-controlling device such as a deformable mirror.

In this chapter, we present a way of how a rotationally symmetric four-zone pupil filter is being designed, to both achieve superresolution property for two different wavelengths. The problems that we face in the design will be carefully discussed in the following pages.



4.2 Basic theory for super-resolution

4.2.1 The 2nd order expansion of the intensity distribution for small displacements of the focus position from geometrical focus

The diffracted intensity distribution near the geometrical focus, while applying the rotationally symmetric amplitude pupil functions, can be analyzed as follows.^[17]

The general complex pupil function can be written as:

$$P(\rho) = T(\rho) \cdot \exp [i\varphi(\rho)] \quad (4.1)$$

where $T(\rho)$ is the transmittance function, and $\phi(\rho)$ is the phase function. Then the normalized complex field amplitude U in the focal region can be written as:

$$U(v, u) = \int_0^1 P(\rho) J_0(v\rho) \exp\left(-\frac{iu\rho^2}{2}\right) \rho d\rho \quad (4.2)$$

Here v and u are radial and axial optical coordinates, respectively

$$v = kr \cdot \sin \alpha; \quad u = 4kz \cdot \sin^2\left(\frac{\alpha}{2}\right); \quad (4.3)$$

Where $\sin \alpha$ is the numerical aperture of the system, and r and z denote the radial and axial distances. In the focal plane, the diffracted field distribution will be:

$$U(v, 0) = 2 \int_0^1 P(\rho) J_0(v\rho) \rho d\rho \quad (4.4)$$

Notice that the above equation is the Hankel transform of the pupil function. Along the axis, we will get:

$$U(0, u) = \int_0^1 P(\rho) \exp\left(-\frac{iu\rho^2}{2}\right) \rho d\rho \quad (4.5)$$

Now we involve the variable $t = \rho^2$, and the pupil function $P(\rho)$ can be written as $Q(t)$.

Then the field distribution along the axis can be written as:

$$U(0, u) = \int_0^1 Q(t) \exp\left(-\frac{iut}{2}\right) dt \quad (4.6)$$

Therefore, it's clear to see that the above equation is the Fourier transform of the equivalent pupil function $Q(t)$. The pupil function is assumed as $P(\rho) = 1$ for the case of achieving the diffraction limit. Somehow, if we carefully modify the pupil function $P(\rho)$, super-resolution can be realized.

According to the theories of Sheppard and Hegedus and De Juan et al. [7], within the 2nd order approximation, the transverse and axial intensity distributions can be expressed as:

$$I(v,0) = |I_0|^2 - \frac{1}{2} \operatorname{Re}(I_0 I_1^*) v^2 \quad (4.7)$$

$$I(0,u) = |I_0|^2 - \operatorname{Im}(I_0^* I_1) u - \frac{1}{4} [\operatorname{Re}(I_2^* I_0) - |I_1|^2] u^2 \quad (4.8)$$

where * denotes the complex conjugate and I_n is the nth moment of the pupil function given by:

$$I_n = 2 \int_0^1 P(\rho) \rho^{2n+1} d\rho \quad (4.9)$$

It can be seen that the transverse intensity is symmetrical with respect to the geometrical focus ($v = 0, u = 0$) [see Appendix B.1]. However, for the axial intensity this is not true in general. The displacement of focus in the axial direction and the Strehl ratio are given by:

$$u_F = -2 \frac{\operatorname{Im}(I_0^* I_1)}{\operatorname{Re}(I_2^* I_0) - |I_1|^2} \quad (4.10)$$

$$S = |I_0|^2 - u_F \operatorname{Im}(I_0^* I_1) \quad (4.11)$$

The transverse and axial gains, which are defined as the ratio between the squared width of the parabolic approximation of the intensity PSF without the filter and with the filter, are given by:

$$G_T = 2 \frac{\operatorname{Re}(I_0 I_1^*) - u_F \operatorname{Im}(I_0^* I_2)}{S} \quad (4.12)$$

$$G_A = 12 \frac{\operatorname{Re}(I_0 I_2^*) - |I_1|^2}{S} \quad (4.13)$$

G_T and G_A are greater than unity for transverse or axial superresolution, respectively.

It should be noted that Eq. 4.10 is valid only for small displacements of the focus position from the geometrical focus, where the second-order expansion of the intensity distribution is a good approximation to describe the focal behavior. The position of the maximum intensity is given by the coordinates $(0, u_F)$. Analogously to the development by Sheppard and Hegedus, expressions for the transverse and axial gains corresponding to complex pupil functions are obtained from the second-order expansion of the intensity with respect to this point.

4.2.2 The 2nd order expansion of the intensity distribution to the case in which the best image plane is not near the paraxial focus

J. Campos, J. C. Escalera, and M. J. Yzuel have extended the expressions for the axial and the transverse gain to the case in which the best image plane is not near the paraxial focus [see Appendix B.2]. They first search for the maximum of the on-axis intensities, and then they develop up to the second order superresolution factors around that point, say u_{\max} . The generalized expressions for those factors are expressed as below:

$$u_0 = -2 \frac{\text{Im}(I_0^* I_1')}{\text{Re}(I_2^* I_0') - |I_1'|^2} \quad (4.14)$$

$$G_T = 2 \frac{\text{Re}(I_0 I_1^*)}{|I_0|^2} \quad (4.15)$$

$$G_A = 12 \frac{\text{Re}(I_0' I_2'^*) - |I_1'|^2}{|I_0'|^2 - \frac{1}{2} u_0 \text{Im}(I_0'^* I_1')} \quad (4.16)$$

$$S = |I_0'|^2 - u_0 \text{Im}(I_0'^* I_1') \quad (4.17)$$

Note that u_0 is measured from the BIP centered at u_{\max} , so its values will be close to zero for most functions of an optical system.

4.2.3 Fourier Optical Transformations

It is necessary for us to give a check to the transverse intensity distributions directly from the basic diffraction theory. The transverse intensity distribution of the image intensity can be obtained by directly convoluting the object intensity distribution function with the point spread function of the optical system. However, it could be a terrible job, implementing the convolution operation [19]. As an alternative choice, we take the Fourier transform of the object intensity distribution function first, and then multiply it with the optical transfer function of the optical system. Next, by taking an inverse Fourier transform of it, the transverse intensity distribution is obtained. Avoiding taking the convolution operation but alternatively implementing the FFT (inverse FFT), it'll help save lots of computing time.

4.3 Structure of Hybrid Dual Focus Lens

A dual focus objective lens of combining aspheric surfaces of DVD and CD for DVD/CD pick-up head has been proposed in 1996 [18].

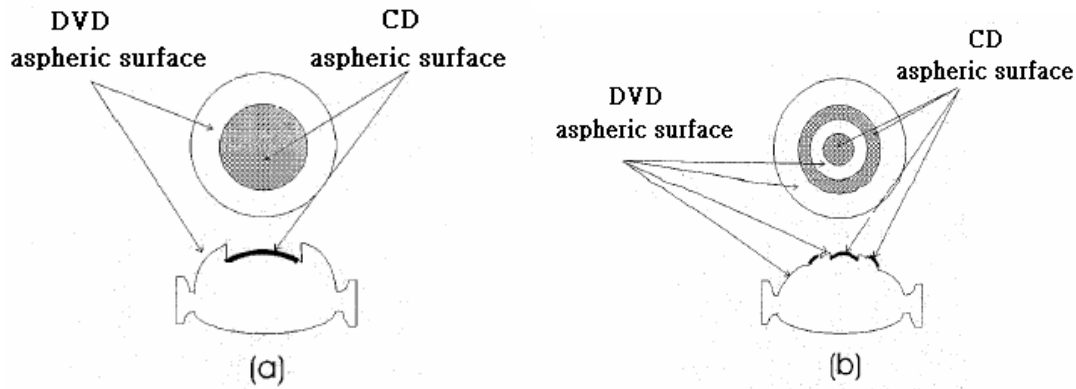


Fig. 4.1 Schematics of (a) the single-ring and (b) the double-ring dual focus lens.

As shown in Fig. 4.1 (a), for a lens consisting of two zones, the CD aspheric surface is located in the central region, while the DVD aspheric surface is located in the outward region. In this way, the objective lens for both CD and DVD can be made into a single lens. However, as a drawback, the lens used in DVD will suffer an obvious side-lobe of the focusing spot. In order to reduce the side-lobe effect of the DVD spot, a four-zone scheme is used, which is shown in Fig. 4.1 (b). The CD aspheric surface portion is composed of the central circle area and the middle zone, while the inner and outward zones form an aspheric surface for DVD lens.

The quality of focus spot of the designed objective lens is a function of the width and position of these zones, which can be numerically calculated based on the scalar diffraction model. Theoretically, the focus spot of DVD and CD can be calculated independently when the focus lengths of DVD and CD are different. Therefore, to calculate the focus spot of DVD, the region of CD is viewed as a mask, and vice versa.

In fig. 4.2, we show the resulting schematic of ray tracing, for which light propagates through a singlet lens with hybrid structure designed for two wavelengths.

The simulated result of the transverse intensity distribution at the focal plane is shown in Fig. 4.3. It tells that the intensity near the optical axis is so strong so that that the effect introduced by the defocusing light can entirely be neglected. This result confirms the validity of making the previous assumptions in the last paragraph.

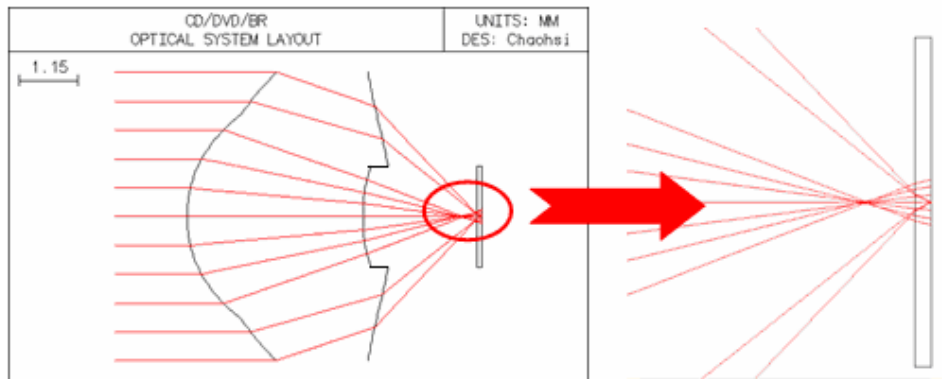


Fig. 4.2 Schematic of the ray trace of a hybrid lens system

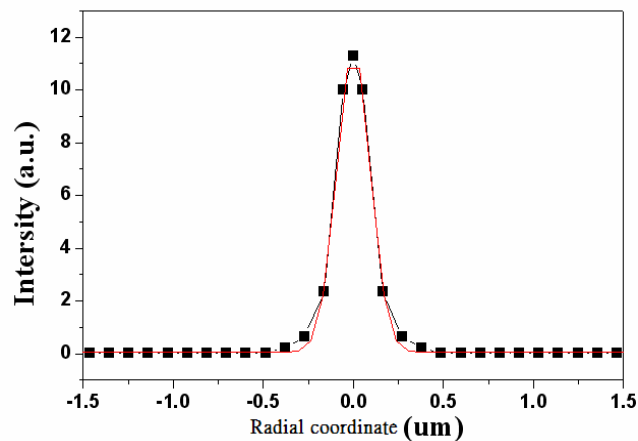


Fig. 4.3 Radial intensity distribution of a hybrid lens system at the focal plane

4.4 Set-up of The Four-zone Pupil Filter

In order to both obtain the super-resolution property for the two DVD/CD wavelengths, the objective lens system is modified by adding a complex pupil filters.

The structure of the complex pupil filter is shown in Fig. 4.4.

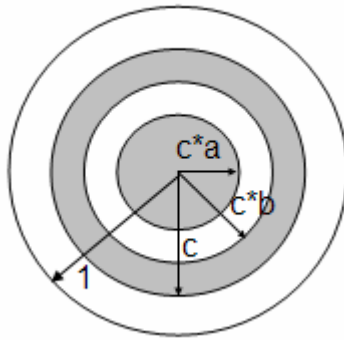


Fig. 4.4 Structure of the four-zone pupil filter

For the portion of CD surface, as shown in Fig. 4.5, since the second zone corresponds to the region of DVD surface, the transmittance of the second zone is assumed to be zero. The transmittances of the first zone and the third zone are assumed to be t_1 and t_3 ; and the corresponding phases of the first zone and the third zone are ϕ_1 and ϕ_3 . The radii are a , b , and 1 . The pupil function for CD can be expressed as:

$$P(\rho) = T(\rho) \cdot \exp[i\varphi(\rho)] = \begin{cases} t_1 \cdot \exp(i\phi_1) & 0 \leq \rho \leq a \\ 0 & a < \rho \leq b \\ t_3 \cdot \exp(i\phi_3) & 0 \leq \rho \leq a \end{cases} \quad (4.18)$$

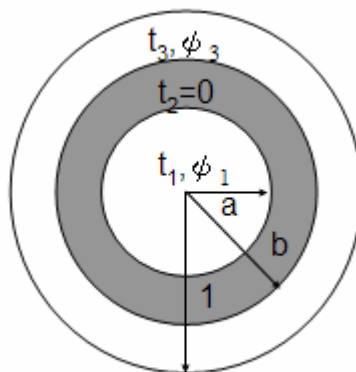


Fig. 4.5 Schematics of the portions of the filter for CD

Then the following moments of the pupil function for CD are obtained:

$$I_0 = t_1 \cdot \exp(i\phi_1) \cdot a^2 + t_3 \cdot \exp(i\phi_3) \cdot (1 - b^2) = a_0 + ib_0 \quad (4.19)$$

$$I_1 = \frac{1}{2} [t_1 \cdot \exp(i\phi_1) \cdot a^4 + t_3 \cdot \exp(i\phi_3) \cdot (1 - b^4)] = a_1 + ib_1 \quad (4.20)$$

$$I_2 = \frac{1}{3} [t_1 \cdot \exp(i\phi_1) \cdot a^6 + t_3 \cdot \exp(i\phi_3) \cdot (1 - b^6)] = a_2 + ib_2 \quad (4.21)$$

For the portion of DVD surface, as shown in Fig. 4.6, since the first and third zone correspond to the region of CD surface, so the transmittance of these two zones are assumed to be zero. The transmittances of the second zone and the fourth zone are T_2 and T_4 ; and the corresponding phases of the second zone and the fourth zone are Ψ_2 and Ψ_4 . The radii are $c \cdot a$, $c \cdot b$, c , and 1 . The pupil function for CD can be expressed as:

$$P(\rho) = T(\rho) \cdot \exp[i\phi(\rho)] = \begin{cases} 0 & 0 \leq \rho \leq c \cdot a \\ T_2 \cdot \exp(i\Psi_2) & c \cdot a < \rho \leq c \cdot b \\ 0 & c \cdot b \leq \rho \leq c \\ T_4 \cdot \exp(i\Psi_4) & c \leq \rho \leq 1 \end{cases} \quad (4.22)$$

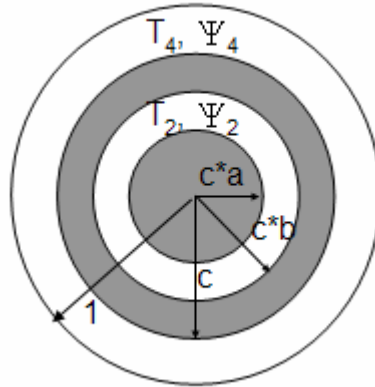


Fig. 4.6 Schematics of the portions of the filter for DVD

Then the following moments of the pupil function for DVD are obtained:

$$I_0 = T_2 \cdot \exp(i\Psi_2) \cdot [(bc)^2 - (ac)^2] + T_4 \cdot \exp(i\Psi_4) \cdot (1 - c^2) = a_0 + ib_0 \quad (4.23)$$

$$I_1 = \frac{1}{2} \{T_2 \cdot \exp(i\Psi_2) \cdot [(bc)^4 - (ac)^4] + T_4 \cdot \exp(i\Psi_4) \cdot (1 - c^4)\} = a_1 + ib_1 \quad (4.24)$$

$$I_2 = \frac{1}{3} \{T_2 \cdot \exp(i\Psi_2) \cdot [(bc)^6 - (ac)^6] + T_4 \cdot \exp(i\Psi_4) \cdot (1 - c^6)\} = a_2 + ib_2 \quad (4.25)$$

Substituting those moments into Eqs. 4.11 and 4.12, the Strehl ratio, the transverse and the axial gains will be expressed as:

$$u_F = \frac{2(a_1b_0 - a_0b_1)}{(a_2a_0 + b_2b_0) - (a_1^2 + b_1^2)} \quad (4.26)$$

$$S = a_0^2 + b_0^2 - u_F(a_0b_1 - a_1b_0) \quad (4.27)$$

$$G_T = 2 \frac{(a_1a_0 + b_1b_0) - u_F(a_0b_2 - a_2b_0)}{S} \quad (4.28)$$

$$G_A = 12 \frac{(a_2a_0 + b_2b_0) - (a_1^2 + b_1^2)}{S} \quad (4.29)$$

On this condition, substituting Eqs. 4.14 and 4.18 into Eqs. 4.4 and 4.5, the expression of the transverse amplitudes for CD and DVD are obtained:

For CD:

$$u(\nu, 0) = \frac{2}{\nu} \{ \exp(i \cdot 0.4\pi) \cdot [J_1(\nu) - b \cdot J_1(a\nu)] + a \cdot J_1(a\nu) \} \quad (4.30)$$

For DVD:

$$u(\nu, 0) = \frac{2}{\nu} \{ \exp(i \cdot 0.35\pi) \cdot [J_1(\nu) - c \cdot J_1(c\nu)] + [cb \cdot J_1(cb \cdot \nu) - ca \cdot J_1(ca \cdot \nu)] \} \quad (4.31)$$

According to

$$I(\nu, 0) = U(\nu, 0) \cdot U^*(\nu, 0) \quad (4.32)$$

Thus, we can obtain the intensity distributions along the transverse direction.

4.5 Illustration and Simulation Verification

4.5.1 Design procedure

The design procedure that we propose here has the following steps:

Step 1:

After carefully setting up all the parameters, like the radius and transmittance of each zone, we use the second order approximation theory, mentioned in section 4.2.1, to calculate the superresolution factors, like the transverse gain, the Strehl ratio, and the displacement of axial focus. Then we can narrow down the range of the parameter in which the wanted superresolution property may be possibly achieved.

Step 2:

To check the accuracy of the computed result gotten in step 1, the transverse intensity distributions are computed directly from the basic diffraction theory without any approximation. We make radial intensity scans at various axial coordinates to find out in where the best image plane (BIP) appears with the applicant the designed filter.

Step 3:

Once the location of the BIP is found, we calculate the gain parameters for the filter in the surrounding of the shifted focus, as what is mentioned in section 4.2.2. Then we fine tune the parameters, like the transmittances of the zones, and observe

the corresponding changes of the superresolution factors.

Step 4:

Similar to the action we list in step two, we give a further check to see if the transverse intensity distributions really achieve transverse superresolution for both wavelengths. If yes, the goal is accomplished.

4.5.2 Simulation Verification

Step 1:

With the condition $a^2+b^2=1$, we adjust the phase factors and the radii of these four zones. For CD surface, t_1 and t_3 are still assigned both to be 1; and φ_1 and φ_3 are assigned to be 0 and 0.4π . For DVD surface, T_2 and T_4 are also assigned both to be 1; and Ψ_2 and Ψ_4 are assigned to be 0 and 0.35π . The value of radius c is first assumed to be 0.7, while the value of radius a varies from 0.4 to 0.6, and the value of radius b is obtained from the relation $b=(1-a^2)^{1/2}$.

With all the factors being settled down, we obtain the relation among the radius a and the transverse gains and Strehl ratio of such a system for both CD and DVD cases, as shown in Fig. 4.7(a) and 4.7(b), respectively. It can be observed that with increase in radius a , the transverse gain decreases for CD, while one increases first and then decreases for DVD. In the range that $a \in [0.4, 0.6]$, the gains are all greater than 1, which means that superresolution property can be realized simultaneously for both CD and DVD. It can also be seen that, for the case of CD, the Strehl ratio increases with the increment of the radius a , but decreases for the case of DVD.

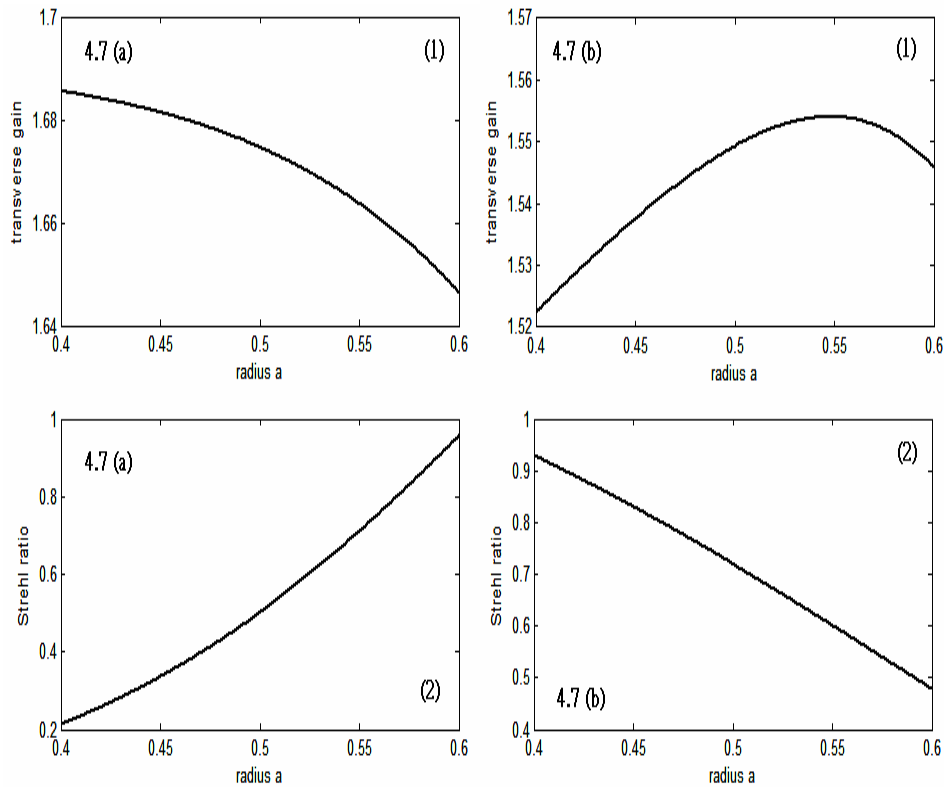


Fig. 4.7: 1) Relation among the transverse gain and the radius of the first zone.

2) Relation among the Strehl ratio and the radius of the first zone.

(a) for the case of CD (b) for the case of DVD

Figures 4.8(a) and 4.8(b), respectively show the transverse intensity distributions for three particular solutions for CD and DVD, corresponding to three different kinds of set-up of the pupil filter, in comparison to the case of clear pupil. The intensity has been normalized to the clear pupil size.

It should be carefully minded that the simulated results of the intensity distribution, shown in Fig. 4.8, disagree with those derived from Eqs. 4.11 and 4.12. For instance, when assuming the value of radius a to be 0.6, the predicted value of the Strehl ratio for CD derived from Eq. 4.11 is about 0.9, while that for DVD is approximately equal to 0.5.

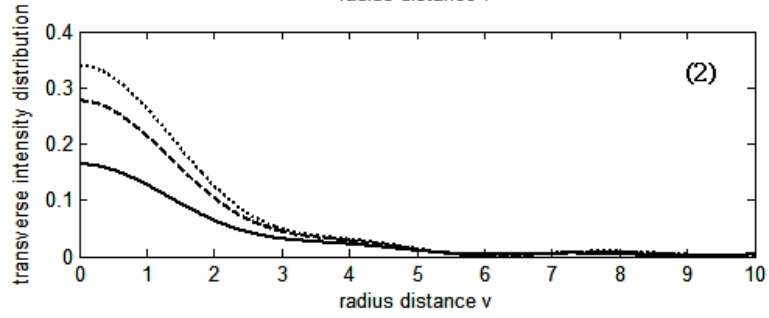
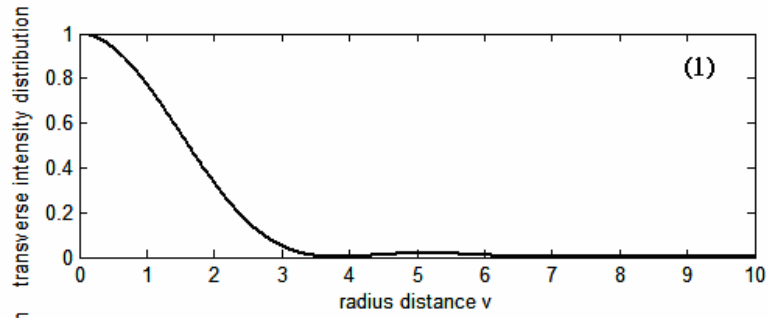


Fig. 4.8(a)

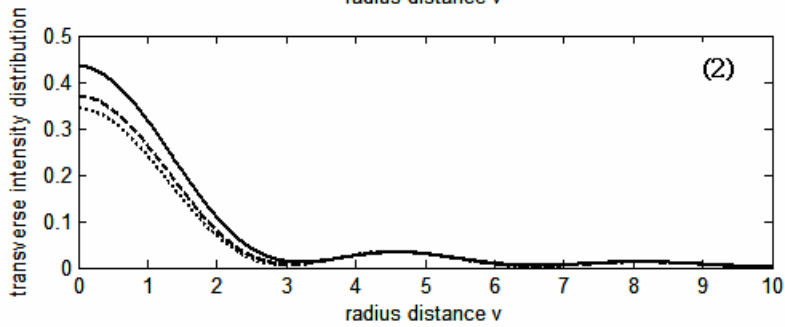
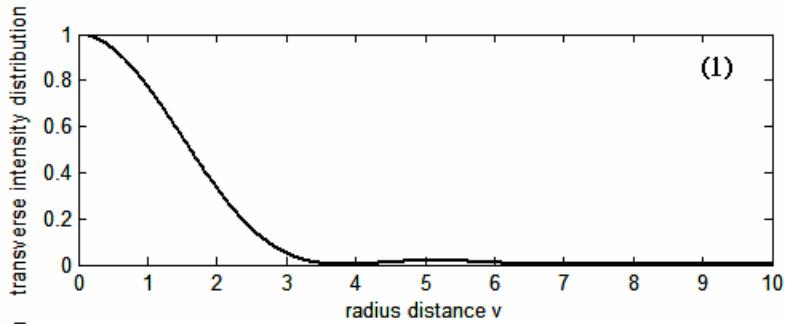


Fig. 4.8(b)

Fig. 4.8: The transverse intensity distributions 1) with the clear pupil, 2) with the designed filter, for $a=0.5$ (solid curve), $a=0.57$ (dashed curve), $a=0.6$ (dotted curve) (a) for the case of CD (b) for the case of DVD.

However, as shown in figure 4.8, the central peak value of the normalized intensity distribution for CD is, in fact, less than 0.4, while that for DVD is less than

0.5. Besides, for CD, the set-up of the filter doesn't achieve the goal of superresolution, but even enlarges the spot size in the focal plane. For DVD, though transverse superresolution is obtained, the transverse side-lobe is tremendously worsened in the focal plane. It is noticed that, for both cases of CD and DVD, the contrast is worsened, which makes it much more difficult in the practical application of reading the data from the disk.

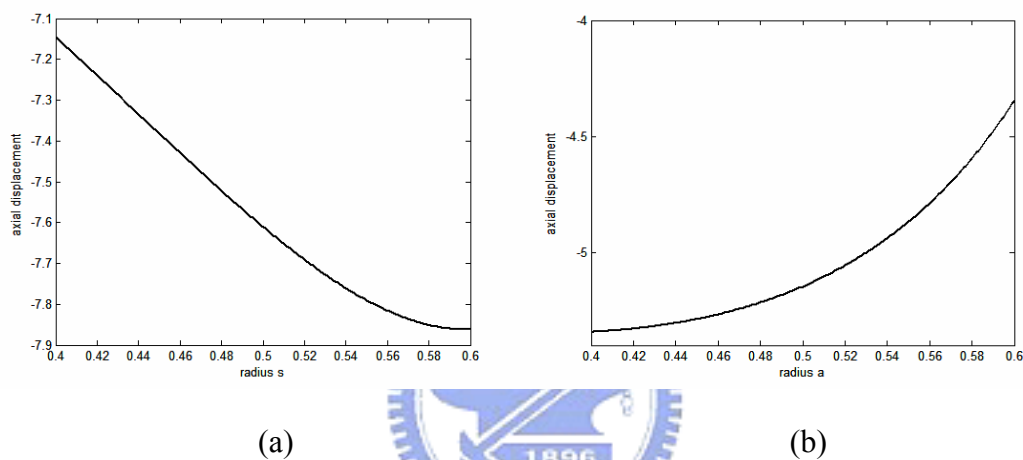


Fig. 4.9: Relation among the displacement of focus in the axial direction and the radius of the first zone. (a) for the case of CD (b) for the case of DVD

It can be clearly be seen in Fig. 4.9 that the computed value of the axial displacement, u_F , is in fact quite apart from zero for both cases of CD and DVD. The place where maxima intensity occurs has been shifted away from the geometric focus, so that the derived forms of Strehl ratio and transverse gain, based on 2nd-order approximation, become incorrect in describing the focal behavior for the designed cases here.

Step 2:

Now, the intensity distributions along the transverse direction for CD and DVD

at the paraxial focus are obtained directly from the computation of the diffraction theory, shown in Fig. 4.10(a) and (b), respectively. We can see that the results correspond to what we have shown in Fig. 4.6. For CD, the goal of superresolution isn't achieved, but even enlarges the spot size; for DVD, though transverse superresolution is obtained, the transverse side-lobe is worsened.

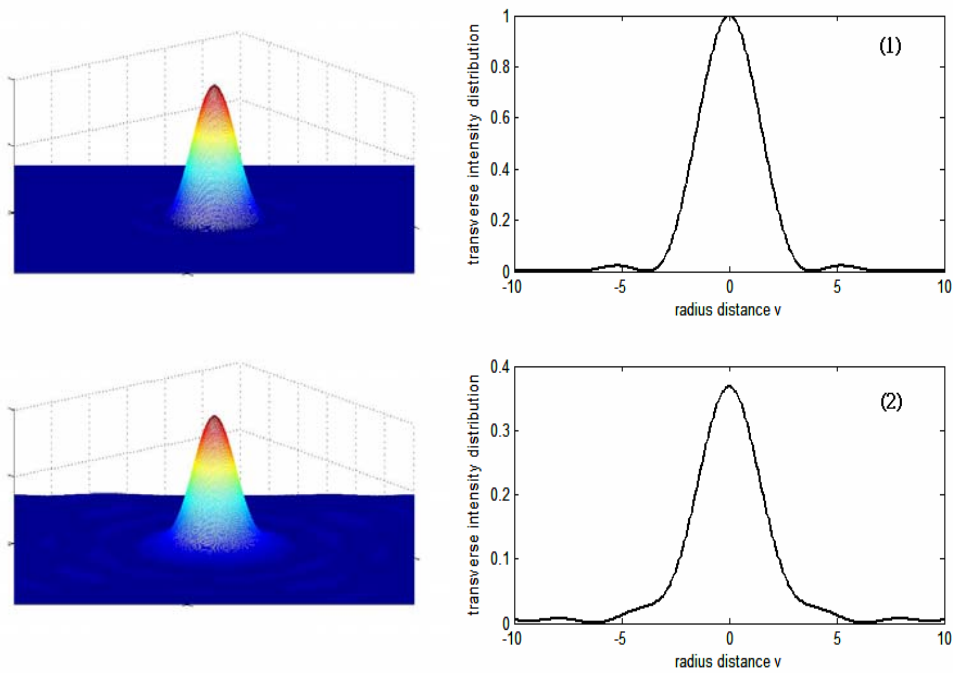


Fig. 4.10 (a)

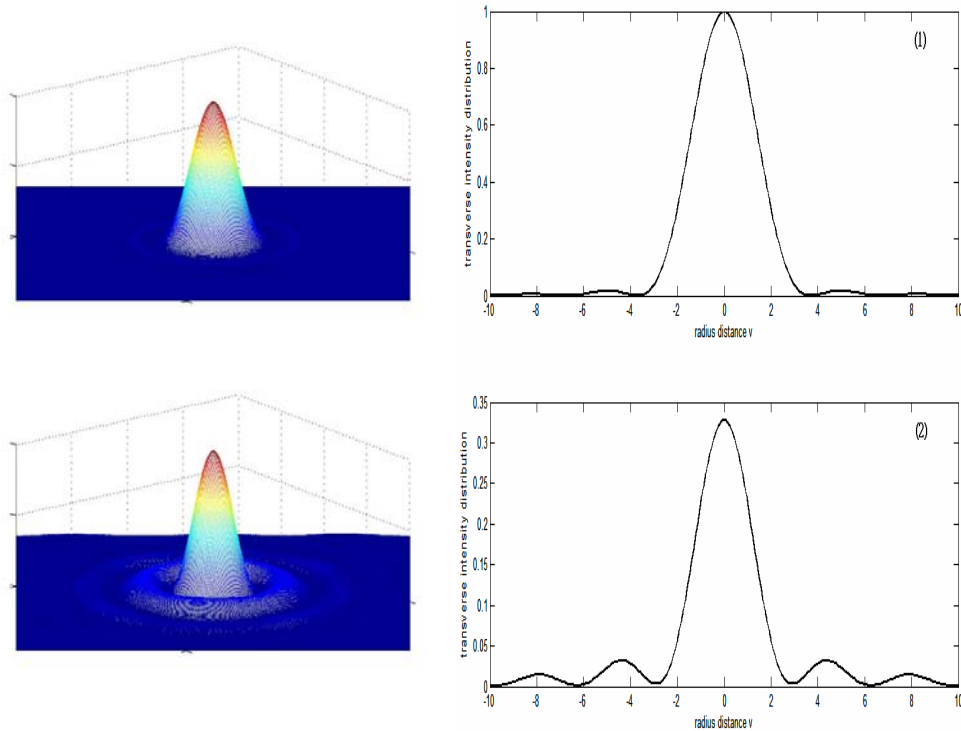


Fig. 4.10(b)

Fig. 4.10: The transverse intensity distributions 1) with the clear pupil, 2) with the designed filter, for $a=0.6$ (a) for the case of CD (b) for the case of DVD.

We are now interested in where the best image plane (BIP) appears after we add the designed filter into the system. Radial intensity scans at various axial coordinates are shown in Fig. 4.11(a) and(b), for CD and DVD, respectively. The range of axial coordinates, u , explored here is -5 to 5, which would certainly seem to cover the transition region we are interested in. From the figure, it seems reasonable to state that the BIP, where best image performance is gotten for both CD and DVD, occurs around $u=3$.

For CD, we can see that the peak value of the main lobe is 0.5 and the side-lobe is extremely small when the radial distance, v , ranges between -10 to 10. The size of blur circle remains the same as the one without adding the filter. For DVD,

transverse superresolution is obtained, but the increased transverse side-lobe will still be a big concern. The contrast of the system performance will be lowered down.

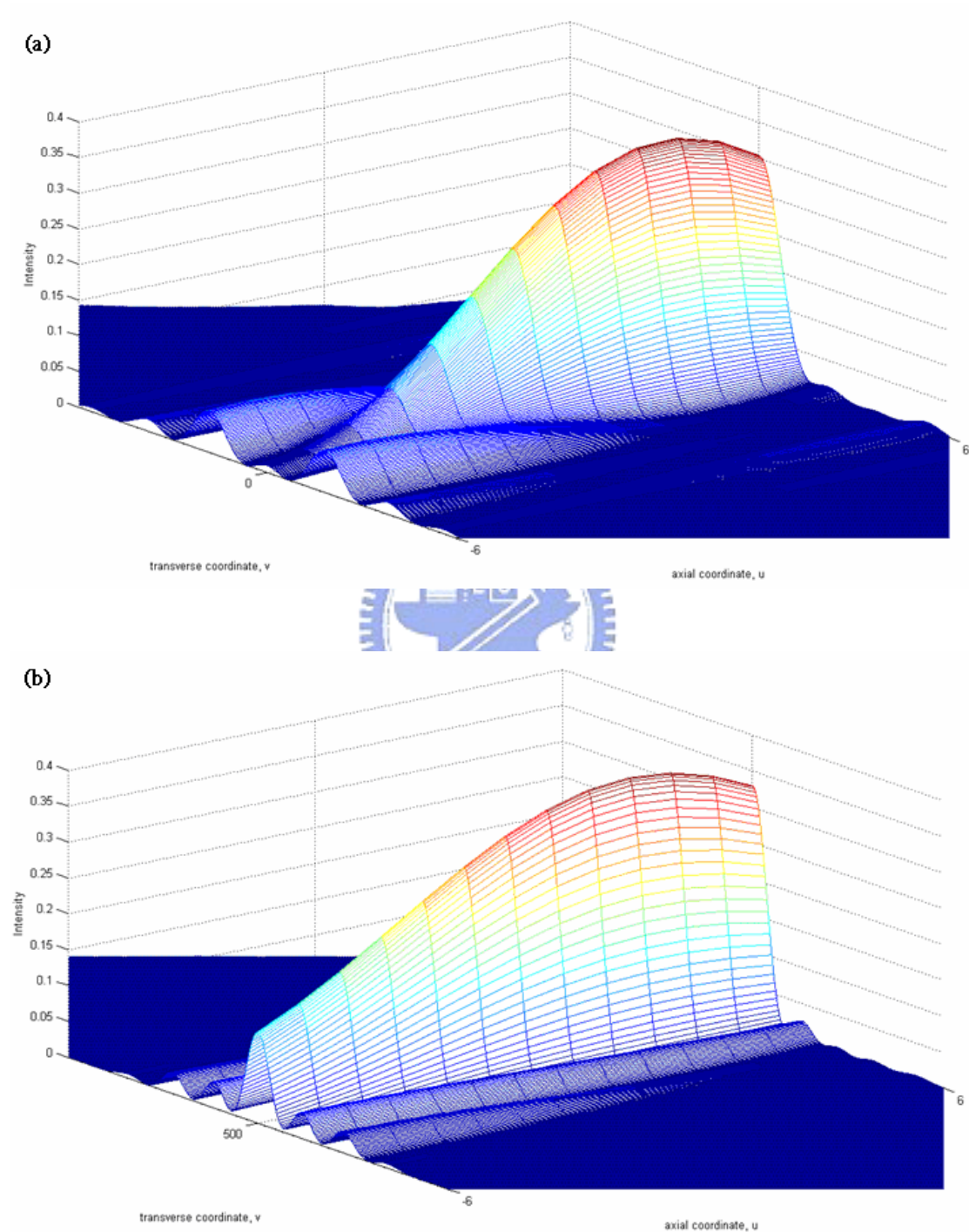


Fig. 4.11: Radial intensity scans at various planes (the range of axial coordinates, u , explored here is -6 to 6) (a) for the case of CD (b) for the case of DVD

Step 3:

When dealing with the case in which the best image plane is not near the paraxial focus, it'll be more proper to use the modified 2nd order approximation method. For CD, we find that the BIP has been shifted to $u=3.527$, while that occurs at $u=3.1$ for DVD. Once the location of the BIP is found, we then fine tune the transmittances of the zones. Here, in this case, we set the transmittance of first zone for CD surface to be 0.7. The computed results of the superresolution factors are shown in Fig. 4.12.

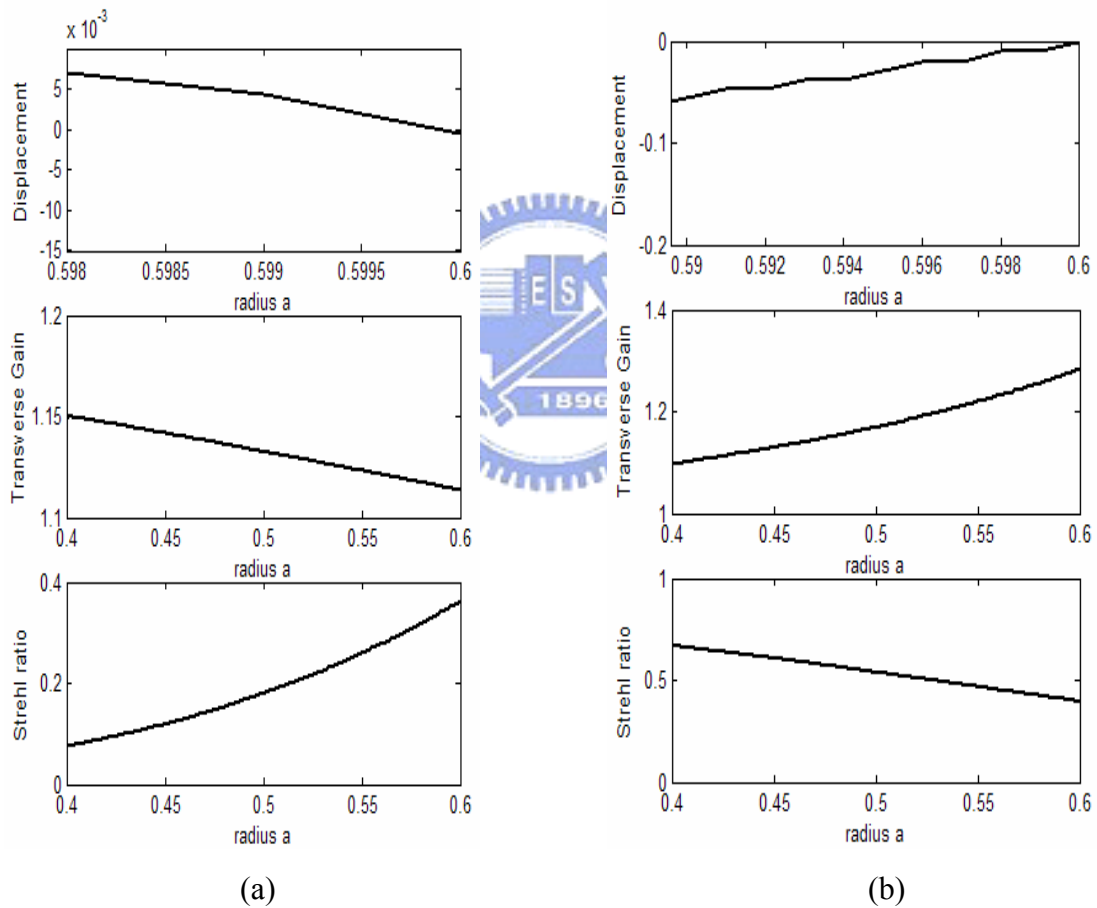


Fig. 4.12: 1) Relation among the displacement and the radius of the first zone.

2) Relation among the transverse gain and the radius of the first zone.

3) Relation among the Strehl ratio and the radius of the first zone.

(a) for the case of CD (b) for the case of DVD

It can be seen that the computed value of the axial displacement is very close to zero when the radius of the first zone is set to be 0.6. The values of transverse gains are all greater than 1 for CD and DVD, which means that superresolution property can be achieved in this case. However, as a drawback, the Strehl ratios for both CD and DVD have dropped greatly, lower than half value of that without a filter.

Step 4:

Similar to what we have done in step 2, now we try to verify the accuracy of the computed results gotten in step 3. The intensity distributions along the transverse direction for CD and DVD at the shifted focus are shown in Fig. 4.13(a) and (b), respectively.

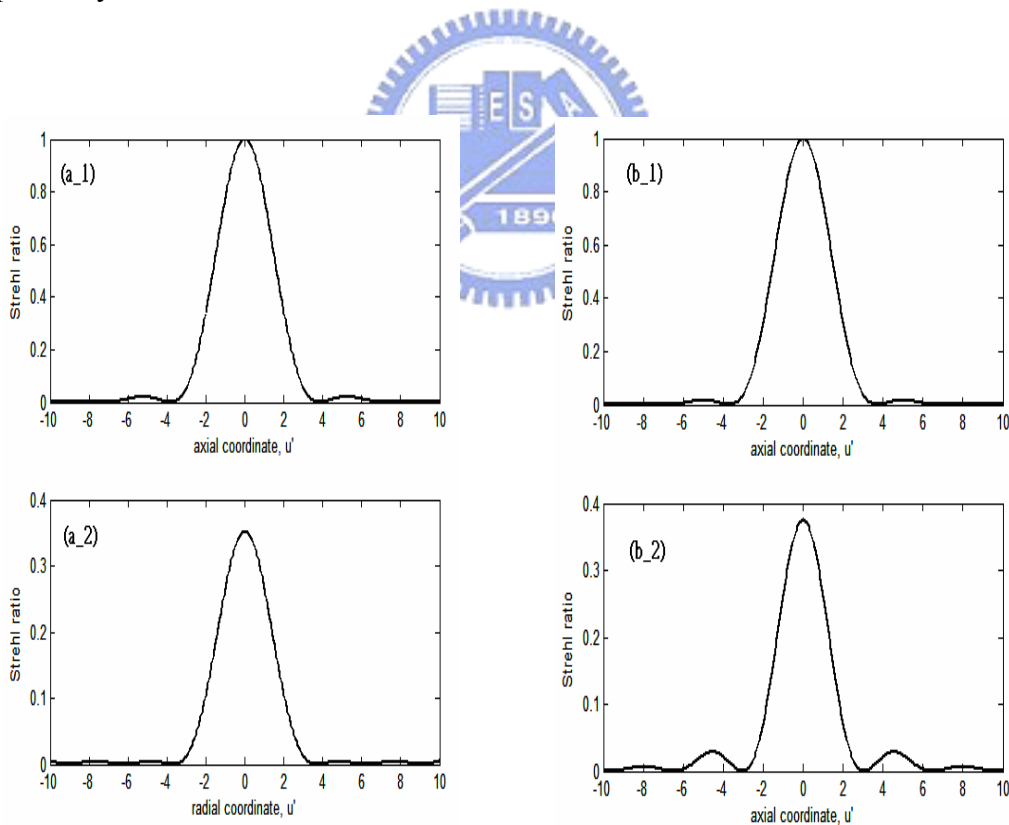


Fig. 4.13 The transverse intensity distributions 1) with the clear pupil, 2) with the designed filter, for radius $a=0.5$; transmittance $t_1= 0.7$ (a) for the case of CD (b) for the case of DVD.

For CD, we find that the transverse gain, in fact, is equal to 1.038, being lower than the expected value; while for DVD, that is equal to 1.259. Besides, the size of the main-lobe of the diffracted pattern has been narrowed down, achieving superresolution in both cases.

Within the range $u' \in [-10, 10]$, we can see that, for CD, the transverse side-lobes become relatively smaller than the central peak value (being approximately 1% of the central peak value). But, for DVD, the transverse side-lobe isn't alleviated but enhanced, which leads to worsen the contrast of the final image.

4.6 Conclusions



In this section, we have shown that, with the use of a rotationally symmetric four-zone pupil filter, transverse superresolution can be both realized for two different wavelengths. Notice that the expressions of the factors, like gains, Strehl ratio, and axial displacement, have to be modified for the case in which the best image plane is not near the paraxial focus. It should also be mentioned that, the transverse sidelobe is somehow troublesome, especially for the case of DVD. In the future work, the main aim in optical superresolution is to reduce the main-lobe size of the point-spread function while increasing the central intensity and suppressing the sidelobes.

Chapter 5

5.1 Conclusions

In the first part of this thesis, we have first presented a radially symmetric phase-only filter to help alleviate the effects caused by the fluctuation of third- and fifth-order spherical aberrations simultaneously. It can be clearly seen that the system tolerance to SA5 is improved by several times. Meanwhile, the trade-off issue, i.e., a reduction in intensity and the MTF, has also been discussed in details. These reductions form the baselines in practical applications of the use of phase filter.

Following the ideas mentioned above, we get interested in seeking a way to enhance the tolerance of the system to defocus or SA3 for both wavelengths. Phase pupil filters used to minimize the variation of Strehl ratio with defocus and third-order spherical aberration (SA3) for dual wavelengths are being discussed. Notice that if the amount of variation of the frequency is small, we may find a form of pupil phase function to achieve that goal.

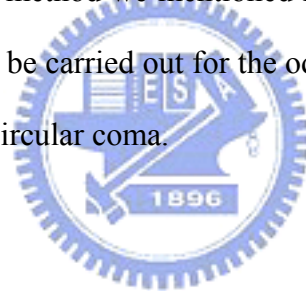
In the last part of this thesis, we have presented a four-zone filter to help achieve transverse superresolution for two different wavelengths, simultaneously. There still

remains some room for improvement. While reducing the main-lobe size of the point-spread function, we need to search for a way to increase the central intensity and suppress the sidelobes.

5.2 Future Work

For the work in Chapter 2:

It's interesting that if we can derive the form of the pupil phase function that extended to even higher order spherical aberration (say, the seventh order spherical aberration, SA7) by using the method we mentioned here. Besides, an investigation similar to that above may also be carried out for the odd-aberration case, i.e., the focal shift, primary and secondary circular coma.



For the work in Chapter 3:

It may be worthwhile of considering the use of hybrid surface lens, an objective lens of combining aspheric surfaces of DVD and CD. In that way, for those two different frequencies, the tolerance of the axial intensity to defocus or SA3 may be simultaneously enhanced.

For the work in Chapter 4:

A global optimization process is needed in the design of the superresolving pupil plate. Once we develop up a reliable optimization method, it'll be much easier for us to find out the best set-up configuration to meet the requirement.

Appendix A: Derivation of The Pupil Phase Functions

A.1 Derivation of the phase filter that has been developed for $W_{040}=W_{020}=0$

By substituting of Eq.(2.9) into Eq.(2.6), it leads to the expression:

$$(\xi^3 + \frac{3}{2}\xi^2 + \frac{3}{4}\xi)\Phi'' - (6\xi + 3)\Phi + [\alpha \cdot (6\xi^4 + 12\xi^3 + 9\xi^2 + \frac{9}{4}\xi) - C \cdot (6\xi + 3)] = 0 \quad (\text{A 1.1})$$

Note that Eq. (A 1.1) is equivalent to the following equation:

$$\frac{d}{d\xi}[a_1(\xi) \cdot \Phi'(\xi) + a_0(\xi) \cdot \Phi(\xi) + a(\xi)] = 0 \quad (\text{A 1.2})$$

where

$$a_1(\xi) = \xi^3 + \frac{3}{2}\xi^2 + \frac{3}{4}\xi \quad (\text{A 1.3})$$

$$a_0(\xi) = -3\xi^2 - 3\xi - \frac{3}{4} \quad (\text{A 1.4})$$

$$a(\xi) = \alpha \cdot (\frac{6}{5}\xi^5 + 3\xi^4 + 3\xi^3 + \frac{9}{8}\xi^2) + C \cdot (-3\xi^2 - 3\xi) + C_1. \quad (\text{A 1.5})$$

The solution of the above equation will be:

$$\Phi(\xi) = \exp[-\int \frac{a_0(\xi)}{a_1(\xi)} d\xi] \cdot \{ [C_2 + C_3 \cdot \int \frac{a(\xi)}{a_1(\xi)} \exp(\int \frac{a_0(\xi)}{a_1(\xi)} d\xi) d\xi] \} \quad (\text{A 1.6})$$

By choosing $\alpha=-5$, $C = -3/8$, and $C_1=0$, a simple solution form will be obtained, which is expressed as:

$$\Phi(\xi) = [(\xi + \frac{1}{2})^3 - \frac{1}{8}] \cdot \{ C_2 + C_3 \cdot \ln[(\xi + \frac{1}{2})^3 - \frac{1}{8}] \} \quad (\text{A 1.7})$$

Note that Eq.(A 1.7) is a particular solution of Eq.(A 1.6), being one of the possible pupil phase functions. With a change of variables, we have the phase pupil function as:

$$\theta(\rho) = \beta_0 (\frac{\rho}{\rho_0})^6 + \beta (\frac{\rho}{\rho_0})^6 \cdot \ln(\frac{\rho}{\rho_0}) \quad (\text{A 1.8})$$

where β and β_0 provide two degrees of freedom and play the role of C_2 and C_3 respectively in Eq.(B 1.7)

A.2 Derivation of the phase filter with Maréchal treatment

By substituting Eq.(2.14) into Eq.(2.6) leads to the expression:

$$[\xi^3 + (B_{26} - \frac{3}{4})\xi]\Phi'' - 6\xi\Phi' + \{\alpha \cdot [6\xi^4 + 6(B_{26} - \frac{3}{4})\xi^2] - C \cdot 6\xi\} = 0 \quad (\text{A 2.1})$$

Note that Eq. (A 2.1) is equivalent to the following equation:

$$\frac{d}{d\xi}[b_1(\xi) \cdot \Phi'(\xi) + b_0(\xi) \cdot \Phi(\xi) + b(\xi)] = 0 \quad (\text{A 2.2})$$

Where

$$b_1(\xi) = \xi^3 + \frac{3}{2}\xi^2 + \frac{3}{4}\xi \quad (\text{A 2.3})$$

$$b_0(\xi) = -3\xi^2 - 3\xi - \frac{3}{4} \quad (\text{A 2.4})$$

$$b(\xi) = \alpha \cdot [\frac{6}{5}\xi^5 + 2(B_{26} - \frac{3}{4})\xi^3] - 3C\xi^2 + C_1\xi + C_2 \quad (\text{A 2.5})$$

The solution of the above equation will be:

$$\Phi(\xi) = \exp[-\int \frac{b_0(\xi)}{b_1(\xi)} d\xi] \cdot \{[\int \frac{b(\xi)}{b_1(\xi)} \exp(\int \frac{b_0(\xi)}{b_1(\xi)} d\xi) d\xi] + C_3\} \quad (\text{A 2.6})$$

For simplicity, let $B_{26}=0.75$ $\alpha=5$, $C=C_1=C_2=0$, we then get the similar form:

$$\Phi(\xi) = \xi^3 [C_3 + C_4 \ln(\xi)] \quad (\text{A 2.7})$$

Notice that $\xi = (\rho / \rho_0)^2 - 1/2$. With a change of variables, the pupil phase function

is expressed as the following form:

$$\theta(\rho) = \beta_0 \left(\frac{\rho}{\rho_0}\right)^6 + \beta \left(\frac{\rho}{\rho_0}\right)^6 \cdot \ln\left(\frac{\rho}{\rho_0}\right) \quad (\text{A 2.8})$$

Appendix B: More Information for 2nd order Approximation Theory

B.1 Further Discussion to The 2nd-order Approximation Theory

We now reexamine the derivation of Eqs. 4.10 to 4.13. As a reminder, in the focal plane, the field distribution can be expressed as [7]:

$$U(\nu, 0) = 2 \int_0^1 P(\rho) J_0(\nu \rho) \rho d\rho \quad (\text{B 1.1})$$

with a change of variable: $t = \rho^2$, we get:

$$U(\nu, 0) = \int_0^1 Q(t) J_0(\nu \sqrt{t}) dt \quad (\text{B 1.2})$$

Notice that the Bessel function of the first kind is expressed as:

$$J_n(x) = \sum_{m=0}^{\infty} \frac{(-1)^m}{m! \Gamma(m+n+1)} \left(\frac{x}{2}\right)^{2m+n} \quad (\text{B 1.3})$$

For small distances from the focus, we can expand the expressions for the focal-plane and axial amplitudes as a power series:

$$U(\nu, 0) = \int_0^1 Q(t) \left(1 - \frac{1}{4} \nu^2 t + \frac{1}{16} \nu^4 t^2 \dots\right) dt \quad (\text{B 1.4})$$

Omitting the higher order terms, we get:

$$U(\nu, 0) = I_0 - \frac{1}{4} \nu^2 I_1 + \frac{1}{16} \nu^4 I_2 \quad (\text{B 1.5})$$

where

$$I_n = \int_0^1 Q(t) t^n dt = 2 \int_0^1 P(\rho) \rho^{2n+1} d\rho \quad (\text{B 1.6})$$

So the transverse (focal) plane intensity will be:

$$I(\nu, 0) = |I_0|^2 - \frac{1}{2} \text{Re}(I_0 I_1^*) \nu^2 \quad (\text{B 1.7})$$

Similarly, the axial intensity will be:

$$I(0, u) = |I_0|^2 - \text{Im}(I_0^* I_1) u - \frac{1}{4} [\text{Re}(I_2^* I_0 - |I_1|^2)] u^2 \quad (\text{B 1.8})$$

B.2 Modification to The Expressions of The Axial and The Transverse Gain

In the recent study, Silvia Ledesma and Juan Campos have extended the expressions for the axial and the transverse gain to the case in which the best image plane is not near the paraxial focus [20]. The content of the study is shown below.

For the case in which the best image plane is not near the paraxial focus, the expressions for the axial gain, transverse gain, and the Strehl ratio need some modifications. Recall that the field along the axis is:

$$U(0, u) = \int_0^1 Q(t) \exp(iut / 2) dt \quad (\text{B 2.1})$$

Where u is the axial coordinate centered at the focal plane without the filter. By evaluating $|U(0, u)|^2$ numerically from Eq. B 2.1, we find the position u_{\max} where the axial intensity is maximum. Then we calculate those factors of superresolution by use of the expansions around this point.

The second-order expansion for the axial response around u_{\max} will be:

$$U(0, u) \cong \int_0^1 Q(t) \exp(iu_{\max} t / 2) [1 + (it / 2)(u - u_{\max}) - (t^2 / 8)(u - u_{\max})^2] dt \quad (\text{B 2.2})$$

The n th moments of the pupil around u_{\max} is defined as:

$$I_n' = 2 \int_0^1 Q(t) t^n \exp(iu_{\max} t / 2) dt \quad (\text{B 2.3})$$

Now the terms taken into account is just up to second order in $u' = u - u_{\max}$, Then the axial intensity is approximated as:

$$I(0, u') \cong |I_0'|^2 - \text{Im}(I_0' I_1'^*) u' + \frac{1}{4} [|I_1'|^2 - \text{Re}(I_0' I_2'^*) u'^2] \quad (\text{B 2.4})$$

For transverse response, we expand the field to second order corresponding to u_{\max} :

$$U(v, u_{\max}) = \int_0^1 Q(t) \left[1 - \frac{1}{4} v^2 t \right] \exp(iu_{\max} t / 2) dt \quad (\text{B 2.5})$$

Then the transverse intensity can be expressed as

$$I(v, u_{\max}) \cong |I_0'|^2 - \frac{1}{2} \text{Re}(I_0' * I_1') v^2 \quad (\text{B 2.6})$$

Note that u_0 corresponds to the center of the parabola defined in Eq. 4.41:

$$u_0 = -2 \frac{\text{Im}(I_0' * I_1')}{\text{Re}(I_2' * I_0') - |I_1'|^2} \quad (\text{B 2.7})$$

Since u_0 is measured from the BIP centered at u_{\max} , so its values will be close to zero for most functions of an optical system. Thus, the superresolution factors around u_{\max} result in:

$$G_T = 2 \frac{\text{Re}(I_0' I_1'^*)}{|I_0'^2|} \quad (\text{B 2.8})$$

$$G_A = 12 \frac{\text{Re}(I_0' I_2'^*) - |I_1'|^2}{|I_0'|^2 - \frac{1}{2} u_0 \text{Im}(I_0' * I_1')} \quad (\text{B 2.9})$$

$$S = |I_0'|^2 - u_0 \text{Im}(I_0' * I_1') \quad (\text{B 2.10})$$

Appendix C: MTLAB Source Codes

C.1: The Strehl ratio as a function of aberration coefficient W_{060}

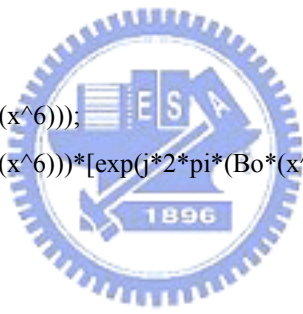
```
% ----- TOPIC: Strehl ratio, S(w20,w40,w60), v.s. W060 ----- %
% ----- Drafted by Chih-Yun Chan, 2nd version, test ok ----- %
% ----- Used in Section 2 ----- %

u1 = zeros(81,1); % Field u1 -- with ideal aperture
u2 = zeros(81,1); % Field u2 -- with the designed filter
I1 = zeros(81,1); % Intensity I1 -- with ideal aperture
I2 = zeros(81,1); % Intensity I2 -- with ideal aperture
B = 7*pi; % assign parameters
Bo = 0.3*7*pi;

% implementing the integral
for i = 0 : 1 : 80
    for x = 0 : 0.001 : 1
        y1 = x*exp(j*2*pi*(((i./10)-4)*(x^6)));
        y2 = x*exp(j*2*pi*(((i./10)-4)*(x^6)))*[exp(j*2*pi*(Bo*(x^6)+B*(x^6)*log(x+1e-6)))]);
        u1(i+1)= u1(i+1)+ 0.001*y1;
        u2(i+1)= u2(i+1)+ 0.001*y2;
    end
end

I1 = u1.*conj(u1)*4*pi*pi/10;
I1 = I1/max(I1); % Normalize the intensity
I2 = u2.*conj(u2)*4*pi*pi/10;
I2 = I2/max(I2); % Normalize the intensity

k = -4 : 0.1 : 4;
plot(k,I1,k,I2)
```



Appendix C: MATLAB Source Codes (CONTINUED)

C.2: Plot of the shape of the designed pupil phase function

```
% ----- TOPIC: The shape of the designed pupil phase function ----- %
% ----- Drafted by Chih-Yun Chan, 1st version, test ok ----- %
% ----- Used in Section 2 ----- %

Th = zeros(1001,1); %Thickness as a function of the radius
B = 5*pi;
Bo = 0.3*B;

for m = 1:1:1001
    Th(m,1)=(Bo*(((m-501)/500)^2)^3)+B*(((m-501)/500)^2)^3*log(((m-501)/500)+1e-8);
end

k=-1:2/1000:1 % Normalized radial coordinate

plot(k,Th);
```



Appendix C: MATLAB Source Codes (CONTINUED)

C.3: Computed MTF with initial setting $W_{020}=0$ and $W_{040}=0$

```

% ----- TOPIC: Computed MTF with initial setting  $W_{020}=0$  and  $W_{040}=0$  ----- %
% ----- Drafted by Chih-Yun Chan, 2nd version, test ok ----- %
% ----- Used in Section 2 ----- %

Q1= zeros(201,201); % Field Q1 -- with  $w_{060}=0$  lambda
Q2= zeros(201,201); % Field Q2 -- with  $w_{060}=0.5$  lambda
Q3= zeros(201,201); % Field Q3 -- with  $w_{060}=1$  lambda
Q4= zeros(201,201); % Field Q4 -- with  $w_{060}=0$  lambda
mtf1 = zeros(80,1); % MTF1 -- with  $w_{060}=0$  lambda
mtf2 = zeros(80,1); % MTF1 -- with  $w_{060}=0$  lambda
mtf3 = zeros(80,1); % MTF1 -- with  $w_{060}=0$  lambda
mtf4 = zeros(80,1); % MTF1 -- with  $w_{060}=0$  lambda
B = 7*pi; % assign parameters
Bo = 0.3*B;

for m = 0:1:200
    for n = 0:1:200
        if(((m-100)*(m-100)+(n-100)*(n-100))<1600)

            Q1(m,n)=exp(j*2*pi*(Bo*(((m-100)/40)^2+((n-100)/40)^2)^3)+B*(((m-100)/40)^2...
                +((n-100)/40)^2)^3*log(((m-100)/40)^2+((n-100)/40)^2)^0.5 +1e-8));

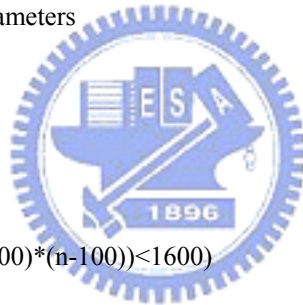
            Q2(m,n)=exp(j*2*pi*(Bo*(((m-100)/40)^2+((n-100)/40)^2)^3)+B*(((m-100)/40)^2...
                +((n-100)/40)^2)^3*log(((m-100)/40)^2+((n-100)/40)^2)^0.5 +1e-8));

            Q3(m,n)=exp(j*2*pi*(Bo*(((m-100)/40)^2+((n-100)/40)^2)^3)+B*(((m-100)/40)^2...
                +((n-100)/40)^2)^3*log(((m-100)/40)^2+((n-100)/40)^2)^0.5 +1e-8));

            Q4(m,n)=exp(j*2*pi*(Bo*(((m-100)/40)^2+((n-100)/40)^2)^3)+B*(((m-100)/40)^2...
                +((n-100)/40)^2)^3*log(((m-100)/40)^2+((n-100)/40)^2)^0.5 +1e-8));

        end
    end
end
end
end

```



```

for m = 0:1:200
    for n = 0:1:200
        if(((m-100)*(m-100)+(n-100)*(n-100))<1600)
            Q1(m,n)=Q1(m,n)*exp(j*2*pi*(((m-100)/40)^2+((n-100)/40)^2)^3)*0);
            Q2(m,n)=Q2(m,n)*exp(j*2*pi*(((m-100)/40)^2+((n-100)/40)^2)^3)*0.5);
            Q3(m,n)=Q3(m,n)*exp(j*2*pi*(((m-100)/40)^2+((n-100)/40)^2)^3)*1);
            Q4(m,n)=Q4(m,n)*exp(j*2*pi*(((m-100)/40)^2+((n-100)/40)^2)^3)*2);
        end
    end
end

otf1=conv2(Q1,conj(Q1));
otf2=conv2(Q2,conj(Q2));
otf3=conv2(Q3,conj(Q3));
otf4=conv2(Q4,conj(Q4));

for n = 1:80
    mtf1(n)=abs(otf1((n+198),199));
    mtf2(n)=abs(otf2((n+198),199));
    mtf3(n)=abs(otf3((n+198),199));
    mtf4(n)=abs(otf4((n+198),199));
end

% Normalization
mtf1= mtf1/max(mtf1);
mtf2= mtf2/max(mtf2);
mtf3= mtf3/max(mtf3);
mtf4= mtf4/max(mtf4);

x1=0:(2/80):(2-2/80);
plot(x1,mtf1,x1,mtf2,x1,mtf3,x1,mtf4)

```



Appendix C: MATLAB Source Codes (CONTINUED)

C.4: Maximal on-axis intensity versus B_{46} .

```
% ----- TOPIC: Maximal on-axis intensity versus  $B_{46}$  ----- %
% ----- Drafted by Chih-Yun Chan, 1st version, test ok ----- %
% ----- Used in Section 2 ----- %

u1 = zeros(161,1); % Field
I1 = zeros(161,1); % Intensity
maxi = zeros(81,1); % Max. intensity v.s.  $B_{46}$ 

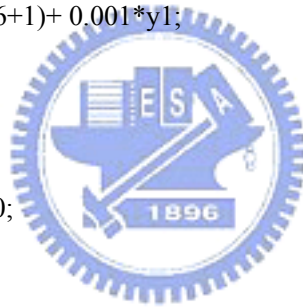
for B46 = 0 : 1 : 80
    for B26 = 0 : 1 : 160
        for x = 0 : 0.001 : 1
            y1 = x*exp(j*2*pi*1*((B26./20 -4)*(x^2)+(B46./20-3.5)*(x^4)+(x^6)));
            u1(B26+1)= u1(B26+1)+ 0.001*y1;
        end
    end
end

I1 = u1.*conj(u1)*4*pi*pi/10;
maxi(B46+1)=max(I1);

u1 = zeros(161,1);
I1 = zeros(161,1);

end

k= -3.5:0.05:0.5;
plot(k,maxi)
```



Appendix C: MATLAB Source Codes (CONTINUED)

C.5: Plot of the Strehl ratio versus B_{26} for different aberration scaling factors f ,

with $B_{46} = -1.5$

```
% ----- TOPIC: Strehl ratio versus  $B_{26}$  for different  $f$ , with  $B_{46} = -1.5$  ----- %
% ----- Drafted by Chih-Yun Chan, 1st version, test ok ----- %
% ----- Used in Section 2 ----- %

u0 = zeros(101,1); u1 = zeros(101,1); u2 = zeros(101,1); u3 = zeros(101,1);
u4 = zeros(101,1); u5 = zeros(101,1); u6 = zeros(101,1); % field with ideal lens

u02 = zeros(101,1); u12 = zeros(101,1); u22 = zeros(101,1); u32 = zeros(101,1);
u42 = zeros(101,1); u52 = zeros(101,1); u62 = zeros(101,1); % field with the filter

I0 = zeros(101,1); I1 = zeros(101,1); I2 = zeros(101,1); I3 = zeros(101,1);
I4 = zeros(101,1); I5 = zeros(101,1); I6 = zeros(101,1); % intensity with ideal lens

I02 = zeros(101,1); I12 = zeros(101,1); I22 = zeros(101,1); I32 = zeros(101,1);
I42 = zeros(101,1); I52 = zeros(101,1); I62 = zeros(101,1); % intensity with the filter

B46=-1.5; % assign parameters
B = 3.9*pi;
Bo = 0.55*B;

for B26 = 0 : 1 : 100 % doing the integration
    for x = 0 : 0.001 : 1

        y0 = x*exp(j*2*pi*0.5*((B26./100)*(x^2)+B46*(x^4)+(x^6)));
        y02 = x*exp(j*2*pi*0.5*((B26./100)*(x^2)+B46*(x^4)...
            +(x^6)))*[exp(j*2*pi*(Bo*(x^6)+B*(x^6)*log(x+1e-6)))]];
        u0(B26+1)= u0(B26+1)+ 0.001*y0;
        u02(B26+1)= u02(B26+1)+ 0.001*y02;

        y1 = x*exp(j*2*pi*1*((B26./100)*(x^2)+B46*(x^4)+(x^6)));
        y12 = x*exp(j*2*pi*1*((B26./100)*(x^2)+B46*(x^4)...
            +(x^6)))*[exp(j*2*pi*(Bo*(x^6)+B*(x^6)*log(x+1e-6)))]];
        u1(B26+1)= u1(B26+1)+ 0.001*y1;
        u12(B26+1)= u12(B26+1)+ 0.001*y12;
    end
end
```

```

+(x^6))*[exp(j*2*pi*(Bo*(x^6)+B*(x^6)*log(x+1e-6)))]];
u1(B26+1)= u1(B26+1)+ 0.001*y1;
u12(B26+1)= u12(B26+1)+ 0.001*y12;

```

```

y2 = x*exp(j*2*pi*2*((B26./100)*(x^2)+B46*(x^4)+(x^6)));
y22 = x*exp(j*2*pi*2*((B26./100)*(x^2)+B46*(x^4)...
+(x^6))*[exp(j*2*pi*(Bo*(x^6)+B*(x^6)*log(x+1e-6)))]];
u2(B26+1)= u2(B26+1)+ 0.001*y2;
u22(B26+1)= u22(B26+1)+ 0.001*y22;

```

```

y3 = x*exp(j*2*pi*3*((B26./100)*(x^2)+B46*(x^4)+(x^6)));
y32 = x*exp(j*2*pi*3*((B26./100)*(x^2)+B46*(x^4)...
+(x^6))*[exp(j*2*pi*(Bo*(x^6)+B*(x^6)*log(x+1e-6)))]];
u3(B26+1)= u3(B26+1)+ 0.001*y3;
u32(B26+1)= u32(B26+1)+ 0.001*y32;

```

```

y4 = x*exp(j*2*pi*4*((B26./100)*(x^2)+B46*(x^4)+(x^6)));
y42 = x*exp(j*2*pi*4*((B26./100)*(x^2)+B46*(x^4)...
+(x^6))*[exp(j*2*pi*(Bo*(x^6)+B*(x^6)*log(x+1e-6)))]];
u4(B26+1)= u4(B26+1)+ 0.001*y4;
u42(B26+1)= u42(B26+1)+ 0.001*y42;

```

```

y5 = x*exp(j*2*pi*5*((B26./100)*(x^2)+B46*(x^4)+(x^6)));
y52 = x*exp(j*2*pi*5*((B26./100)*(x^2)+B46*(x^4)...
+(x^6))*[exp(j*2*pi*(Bo*(x^6)+B*(x^6)*log(x+1e-6)))]];
u5(B26+1)= u5(B26+1)+ 0.001*y5;
u52(B26+1)= u52(B26+1)+ 0.001*y52;

```

```

y6 = x*exp(j*2*pi*6*((B26./100)*(x^2)+B46*(x^4)+(x^6)));
y62 = x*exp(j*2*pi*6*((B26./100)*(x^2)+B46*(x^4)...
+(x^6))*[exp(j*2*pi*(Bo*(x^6)+B*(x^6)*log(x+1e-6)))]];
u6(B26+1)= u6(B26+1)+ 0.001*y6;
u62(B26+1)= u62(B26+1)+ 0.001*y62;

```

```
end
```

```
end
```

```
I0 = u0.*conj(u0)*4*pi*pi/10;
```

```
I1 = u1.*conj(u1)*4*pi*pi/10;  
I2 = u2.*conj(u2)*4*pi*pi/10;  
I3 = u3.*conj(u3)*4*pi*pi/10;  
I4 = u4.*conj(u4)*4*pi*pi/10;  
I5 = u5.*conj(u5)*4*pi*pi/10;  
I6 = u6.*conj(u6)*4*pi*pi/10;
```

```
I02 = u02.*conj(u02)*4*pi*pi/10;  
I12 = u12.*conj(u12)*4*pi*pi/10;  
I22 = u22.*conj(u22)*4*pi*pi/10;  
I32 = u32.*conj(u32)*4*pi*pi/10;  
I42 = u42.*conj(u42)*4*pi*pi/10;  
I52 = u52.*conj(u52)*4*pi*pi/10;  
I62 = u62.*conj(u62)*4*pi*pi/10;
```

```
k = 0 : 0.01 : 1.0;
```

```
plot(k,I12,k,I22,k,I32,k,I42,k,I52,k,I62)
```



Appendix C: MATLAB Source Codes (CONTINUED)

C.6: The Strehl ratio as a function of aberration scaling factor f , with

$B_{26} = 0.6$ and $B_{46} = -1.5$.

```
% ----- TOPIC: Strehl ratio as a function of  $f$ , with  $B_{26} = 0.6$  and  $B_{46} = -1.5$ . ----- %
% ----- Drafted by Chih-Yun Chan, 2nd version, test ok ----- %
% ----- Used in Section 2 ----- %

u1 = zeros(101,1); % field with ideal lens
u2 = zeros(101,1); % field with the phase filter
I1 = zeros(101,1); % intensity with ideal lens
I2 = zeros(101,1); % intensity with the phase filter

B46=-1.5; % assign parameters
B = 5*pi;
Bo = 0.3*B;

for f = 0 : 1 : 100 % doing the integration
    for x = 0 : 0.001 : 1
        y1 = x*exp(j*2*pi*f/10*(0.6*(x^2)+B46*(x^4)+(x^6)))...
            *[exp(j*2*pi*(Bo*(x^6)+B*(x^6)*log(x+1e-6)))]);
        y2 = x*exp(j*2*pi*f/10*(0.6*(x^2)+B46*(x^4)+(x^6)));
        u1(f+1)= u1(f+1)+ 0.001*y1;
        u2(f+1)= u2(f+1)+ 0.001*y2;
    end
end

I1 = u1.*conj(u1)*4*pi*pi/10;
I1= I1/max(I1); % Normalization
I2 = u2.*conj(u2)*4*pi*pi/10;
I2= I2/max(I2); % Normalization

k = 0 : 0.1 : 10;
plot(k,I1,k,I2)
```

Appendix C: MATLAB Source Codes (CONTINUED)

C.7: 1) Relation among the transverse gain and the radius of the first zone.

2) Relation among the Strehl ratio and the radius of the first zone

-- For CD

```

% -----      TOPIC:  SR v.s. radius a; GT v.s. radius a  (for CD)  ----- %
% -----      Drafted by Chih-Yun Chan, 2nd version, test ok  ----- %
% -----      Used in Section 4  ----- %

double NUM;      % number of points in the interval a: 0.4~0.6
double a(NUM+1); % radius of the 1st zone
double b(NUM+1); % radius of the 2nd zone
double t1;       % transmission of zone 1
double t2;       % transmission of zone 3
double phi;      % phase difference of the zones
double I0(NUM+1); double a0(NUM+1); double b0(NUM+1);
double I1(NUM+1); double a1(NUM+1); double b1(NUM+1);
double I2(NUM+1); double a2(NUM+1); double b2(NUM+1);
double uF(NUM+1);
double SR(NUM+1);
double GT(NUM+1);
double GA(NUM+1);

t1= 1;          % assign the parameters
t2= 1;
phi=0.4
NUM = 200;

for i = 0 : NUM
    a(i+1) = 0.4 + (0.2/NUM). *i;
    b(i+1) = sqrt(1-a(i+1). *a(i+1));
    I0(i+1) = exp(j*0*pi)*(t1. *(a(i+1).^2)) + t2. *exp(j*phi*pi)*(1-(b(i+1).^2));
    a0(i+1) = real(I0(i+1));
    b0(i+1) = imag(I0(i+1));
    I1(i+1) = 0.5*exp(j*0*pi)*(t1. *(a(i+1).^4)) + t2. *0.5*exp(j*phi*pi)*(- (b(i+1).^4) +1);
    a1(i+1) = real(I1(i+1));
    b1(i+1) = imag(I1(i+1));
    I2(i+1) = (1/3)*exp(j*0*pi)*(t1. *(a(i+1).^6))+ t2. *(1/3)*exp(j*phi*pi)*(- (b(i+1).^6) +1);
    a2(i+1) = real(I2(i+1));

```



```
b2(i+1) = imag(I2(i+1));
```

```
% the displacement of the focus
```

```
uF(i+1) = 2*(a1(i+1).*b0(i+1)-a0(i+1).*b1(i+1))./( (a2(i+1).*a0(i+1)+b2(i+1).*b0(i+1))...  
- (a1(i+1).*a1(i+1)+b1(i+1).*b1(i+1)) );
```

```
% the Strehl ratio
```

```
SR(i+1) = a0(i+1).*a0(i+1) + b0(i+1).*b0(i+1)...  
- uF(i+1).*(a0(i+1).*b1(i+1)-a1(i+1).*b0(i+1));
```

```
% the transverse gain
```

```
GT(i+1) = 2*( (a1(i+1).*a0(i+1)+b0(i+1).*b1(i+1))...  
- uF(i+1).*(-a2(i+1).*b0(i+1)+a0(i+1).*b2(i+1)) )./SR(i+1);
```

```
% the axial gain
```

```
GA(i+1) = 12*( (a2(i+1).*a0(i+1)+b0(i+1).*b2(i+1))...  
- (a1(i+1).*a1(i+1)+b1(i+1).*b1(i+1)) )./SR(i+1);
```

```
end
```

```
m = 0.4: (0.2/NUM): 0.6;  
subplot(2,1,1); plot(m,uF);  
subplot(2,1,2); plot(m,SR);
```



Appendix C: MATLAB Source Codes (CONTINUED)

C.8: 1) Relation among the transverse gain and the radius of the first zone.

2) Relation among the Strehl ratio and the radius of the first zone

-- For DVF

```
% ----- TOPIC: SR v.s. radius a; GT v.s. radius a (for DVD) ----- %
% ----- Drafted by Chih-Yun Chan, 2nd version, test ok ----- %
% ----- Used in Section 4 ----- %

double NUM; % number of points in the interval a: 0.4~0.6
double a(NUM+1); % radius of the 1st zone
double b(NUM+1); % radius of the 2nd zone
double t1; % transmission of zone 2
double t2; % transmission of zone 4
double phi; % phase difference of the zones
double I0(NUM+1); double a0(NUM+1); double b0(NUM+1);
double I1(NUM+1); double a1(NUM+1); double b1(NUM+1);
double I2(NUM+1); double a2(NUM+1); double b2(NUM+1);
double uF(NUM+1);
double SR(NUM+1);
double GT(NUM+1);
double GA(NUM+1);

c= 0.7; % assign parameters
t1=1;
t2=1;
phi=0.35;
NUM = 200;

for i = 0 : NUM
    a(i+1) = 0.4 + (0.2/NUM).*i;
    b(i+1) = sqrt(1-a(i+1).*a(i+1));
    I0(i+1) = t1.*exp(j*0*pi)*((c.*b(i+1)).^2-(c.*a(i+1)).^2) + t2.*exp(j*phi*pi)*(1-(c).^2);
    a0(i+1) = real(I0(i+1));
    b0(i+1) = imag(I0(i+1));
    I1(i+1) = (1/2)*(t1.*exp(j*0*pi)*((c.*b(i+1)).^4-(c.*a(i+1)).^4) + t2.*exp(j*phi*pi)*(1-(c).^4));
    a1(i+1) = real(I1(i+1));
```

```

b1(i+1) = imag(I1(i+1));
I2(i+1) = (1/3)*(t1.*exp(j*0*pi)*((c.*b(i+1)).^6-(c.*a(i+1)).^6) + t2.*exp(j*phi*pi)*(1-(c).^6));
a2(i+1) = real(I2(i+1));
b2(i+1) = imag(I2(i+1));

% the displacement of the focus
uF(i+1) = 2*(a1(i+1).*b0(i+1)-a0(i+1).*b1(i+1))...
        ./((a2(i+1).*a0(i+1)+b2(i+1).*b0(i+1)) - (a1(i+1).*a1(i+1)+b1(i+1).*b1(i+1)));

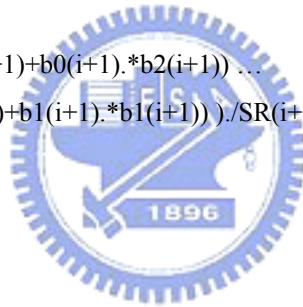
% the Strehl ratio
SR(i+1) = a0(i+1).*a0(i+1) + b0(i+1).*b0(i+1) - uF(i+1).*(a0(i+1).*b1(i+1)-a1(i+1).*b0(i+1));

% the transverse gain
GT(i+1) = 2*( (a1(i+1).*a0(i+1)+b0(i+1).*b1(i+1))...
        - uF(i+1).*(-a2(i+1).*b0(i+1)+a0(i+1).*b2(i+1)) )./SR(i+1);

% the axial gain
GA(i+1) = 12*( (a2(i+1).*a0(i+1)+b0(i+1).*b2(i+1)) ...
        -(a1(i+1).*a1(i+1)+b1(i+1).*b1(i+1)) )./SR(i+1);
end

m = 0.4: (0.2/NUM): 0.6;
%subplot(2,1,1);
plot(m,uF);
%subplot(2,1,2); plot(m,SR);

```



Appendix C: MATLAB Source Codes (CONTINUED)

C.9: The transverse intensity distributions -- For CD

```

% ----- TOPIC: the transverse intensity distributions (for CD) ----- %
% ----- Drafted by Chih-Yun Chan, 2nd version, test ok ----- %
% ----- Used in Section 4 ----- %

v = (0:0.01:10)'; % radius distance
double a(3); % radius of the 1st zone
double b(3); % radius of the 2nd zone
double U(1001,3); % field with the clear aperture
double Ut(1001,3); % field with the designed filter
double I(1001,3); % intensity with the clear aperture
double It(1001,3); % intensity with the designed filter

a(1)=0.5; a(2)=0.57; a(3)=0.6;
b(1)=sqrt(1-a(1).*a(1)); b(2)=sqrt(1-a(2).*a(2)); b(3)=sqrt(1-a(3).*a(3));

warning off;

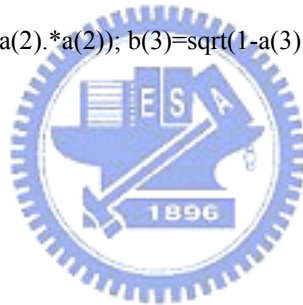
for k = 1:3
    for i = 0 : 1000
        U(i+1,k) = (2./v(i+1))*besselj(1,v(i+1));
        Ut(i+1,k) = (2./v(i+1))*( a(k).*besselj(1,(a(k).*v(i+1)))...
            + exp(j*0.1*pi).*( besselj(1,v(i+1)) - b(k).*besselj(1,(b(k).*v(i+1))) ) ) );
    end
end

for k= 1:3
    I(1:1001,k) = U(1:1001,k).*conj(U(1:1001,k));
    It(1:1001,k) = Ut(1:1001,k).*conj(Ut(1:1001,k));
end

subplot(2,1,1); plot(v,I(:,1),v,I(:,2),v,I(:,3));
subplot(2,1,2); plot(v,It(:,1),v,It(:,2),v,It(:,3));

warning on;

```



Appendix C: MATLAB Source Codes (CONTINUED)

C.10: The transverse intensity distributions -- For DVD

```

% ----- TOPIC: the transverse intensity distributions (for DVD) ----- %
% ----- Drafted by Chih-Yun Chan, 2nd version, test ok ----- %
% ----- Used in Section 4 ----- %

v = (0:0.01:10)'; % radius distance
double a(3); % radius of the 1st zone
double b(3); % radius of the 2nd zone
double U(1001,3); % field with the clear aperture
double Ut(1001,3); % field with the designed filter
double I(1001,3); % intensity with the clear aperture
double It(1001,3); % intensity with the designed filter

a(1)=0.5; a(2)=0.57; a(3)=0.6;
b(1)=sqrt(1-a(1).*a(1)); b(2)=sqrt(1-a(2).*a(2)); b(3)=sqrt(1-a(3).*a(3));
c=0.7;

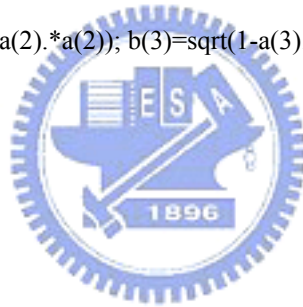
warning off;

for k = 1:3
    for i = 0 : 1000
        U(i+1,k) = (2./v(i+1))*besselj(1,v(i+1));
        Ut(i+1,k) = (2./v(i+1))*( c.*b(k).*besselj(1,(c.*b(k).*v(i+1)))...
            -c.*a(k).*besselj(1,(c.*a(k).*v(i+1)))...
            + exp(j*0.35*pi).*(besselj(1,v(i+1))-c.*besselj(1,(c.*v(i+1))) ) );
    end
end

for k= 1:3
    I(1:1001,k) = U(1:1001,k).*conj(U(1:1001,k));
    It(1:1001,k) = Ut(1:1001,k).*conj(Ut(1:1001,k));
end

subplot(2,1,1); plot(v,I(:,1),v,I(:,2),v,I(:,3));
subplot(2,1,2); plot(v,It(:,1),v,It(:,2),v,It(:,3));
warning on;

```



Appendix C: MATLAB Source Codes (CONTINUED)

C.11: Radial intensity scans at various planes (FFT method)

```
% ----- TOPIC: Radial intensity scans at various planes (FFT) ----- %
% ----- Drafted by Chih-Yun Chan, 2nd version, test ok ----- %
% ----- Used in Section 4 ----- %

sq=zeros(1000); % field with the clear aperture
sq1=zeros(1000); % field with the designed fillter
double u;
u = 3;
for m = 0 : 1 : 1000 % generate the pupil function
    for n = 0 : 1 : 1000
        if(((m-500)*(m-500)+(n-500)*(n-500))^0.5<10*0.6)
            sq1((m+1),(n+1))=1*exp(-j*u*((m-500)*(m-500)+(n-500)*(n-500))/2/100);
        end

        if(((m-500)*(m-500)+(n-500)*(n-500))^0.5>10*(sqrt(1-0.6*0.6)))
            if(((m-500)*(m-500)+(n-500)*(n-500))^0.5<10)
                sq1((m+1),(n+1))=exp(j*0.35*pi)*...
                    exp(-j*u*((m-500)*(m-500)+(n-500)*(n-500))/2/100);
            end
        end
    end

    if(((m-500)*(m-500)+(n-500)*(n-500))^0.5<10)
        sq((m+1),(n+1))=1;
    end
end

end

sqft=fftshift(fft2(fftshift(sq)));
sqft1=fftshift(fft2(fftshift(sq1)));
I=sqft.*conj(sqft);
I1=sqft1.*conj(sqft1);

k= -500*1.22*pi/61: 1.22*pi/61 : 1.22*pi/61*499;
subplot(2,1,1); plot(k,(I(:,501)./max(I(:,501))));
subplot(2,1,2); plot(k,(I1(:,501)./max(I1(:,501))));
```


Bibliography (Section 2)

- 2.1. W. T. Welford, *Aberrations of Optical Systems*, (Adam Hilger, New York, 1986)
- 2.2. V. N. Mahajan, *Optical Imaging and Aberration*, (SPIE Optical Engineering Press, Bellingham, Wash., 1998)
- 2.3. J. Campos, J. Escalera and M. J. Yzuel, "Symmetry properties with pupil phase-filters," *Opt. Express* **12**, 2548-2559 (2004)
- 2.4. A. Castro and J. Ojeda-Castaneda, "Asymmetric masks for extended depth of field," *Appl. Opt.* **43**, 3474-3479 (2004)
- 2.5. E. R. Dowski, Jr., and W. T. Cathey, "Extended depth of field through wave-front coding," *Appl. Opt.* **34**, 1859-1866 (1995)
- 2.6. H. Wang and F. Gan, "High focal depth with a pure-phase apodizer," *Appl. Opt.* **40**, 5658-5662 (2001)
- 2.7. H. Wang and F. Gan, "Phase-shifting apodizers for increasing focal depth," *Appl. Opt.*, **41**, 5263-5266 (2002)
- 2.8. N. George and W.-L. Chi, "Extended depth of field using a logarithmic asphere," *J. Opt. A- Pure Appl. Opt.* **5**, S157-S163 (2003)
- 2.9. D. Zalvidea and E. E. Sicre, "Phase pupil functions for focal-depth enhancement derived from a Wigner distribution function," *Appl. Opt.* **37**, 3623-3627 (1998)
- 2.10. S. Mezouari and A.R. Harvey, "Phase pupil functions for reduction of defocus and spherical aberrations," *Opt. Lett.* **28**, 771-773 (2003)
- 2.11. V. A. Borovikov, *Uniform Stationary Phase Method*, (Institution of Electrical Engineers, London, 1994)
- 2.12. A. Walther, *The Ray and Wave Theory of Lenses*, (Cambridge University Press, New York, 1995). pp.154-165,
- 2.13. OSLO Optics Reference (Release 6.1), pp.104-119; available from Lambda Research Corp. (can be downloaded from <http://www.lambdare.com>)

Bibliography (Section 2 Continued)

- 2.14. A. Maréchal, "Study of the combined effects of diffraction and geometrical aberrations on the image of a luminous point," *Rev d'Optique*, **26**, 257-77 (1947)
- 2.15. M. Born and E. Wolf, *Principle of Optics*, (Cambridge University Press, New York, 1999), p.468,
- 2.16. W. B. King, "Dependence of the Strehl Ratio on The Magnitude of the Variance of the Wave Aberration," *J. Opt. Soc. Am.*, **58**, 655-661, (1968)

Bibliography (Section 3)

- 3.1 Wang, Z. Chen, and F. Gan, "High Focal Depth with a Pure-Phase Apodizer", *Appl. Opt.* **40**, 5658-5662 (2001)
- 3.2 X. Gao, Z Fei, W. Xu, F. Gan, "Focus splitting induced by a pure phase-shifting apodizer," *Opt. Comm.* **239**, 55-59(2004)"
- 3.3 A. R. FitzGerrell, E. R. Dowski, Jr., and W. T Cathey, "Defocus transfer function for circularly symmetric pupils," *Appl. Opt.*, 5796-5804 (1997)
- 3.4 A. Walther, *The Ray and Wave Theory of Lenses*, (Cambridge, 1995)
- 3.5 W. T. Welford, FRS, *Aberrations of Optical Systems*, (Adam Hilger Ltd, 1986)
- 3.6 V. N. Mahajan, *Optical Imaging and Aberration*, (SPIE Optical Engineering Press, Bellingham, Wash., 1998)
- 3.7 V. N. Mahajan, *Aberration Theory Made Simple*, (SPIE, 1991)
- 3.8 OSLO Optics Reference (Release 6.1), pp.104-119; available from Lambda Research Corp. (can be downloaded from <http://www.lambdare.com>)

Bibliography (Section 4)

- 4.1 G. Toraldo di Francia, "Super-gain antennas and optical resolving power," *Nuovo Cimento, Suppl.* **9**, 426-435 (1952)

Bibliography (Section 4 Continued)

- 4.2 T. R. M. Sales and G. M. Morris, “Diffractive superresolution element,” *J. Opt. Soc. Am. A* **24**, 2637 (1997)
- 4.3 T. R. M. Sales and G. M. Morris, ” Fundamental limits of optical superresolution,” *Opt. Lett.* **9**, 582-584 (1997)
- 4.4 G. Boyer, “New class of axially apodizing filters for confocal scanning microscopy,” *J. Opt. Soc. Am. A* **19**, 584–589 (2002)
- 4.5 M. Gu, T. Tannous, and C. J. R. Sheppard, “Effect of an annular pupil on confocal imaging through highly scattering media,” *Opt. Lett.* **21**, 312–314 (1995)
- 4.6 C. J. R. Sheppard, “Leaky annular pupils for improved axial imaging,” *Optik (Stuttgart)* **99**, 32–34 (1995)
- 4.7 C. J. R. Sheppard and Z. S. Hegedus, “Axial behavior of pupil plane filters,” *J. Opt. Soc. Am. A* **5**, 643–647 (1988)
- 4.8 D. M. de Juana, J. E. Oti, V. F. Canales, and M. P. Cagigal, “Transverse or axial superresolution in a 4Pi-confocal microscope by phase-only filters,” *J. Opt. Soc. Am. A* **20**, 2172–2178 (2003)
- 4.9 T. R. M. Sales and G. M. Morris, “Axial superresolution with phase-only pupil filters,” *Opt. Commun.* **156**, 227–230, (1998).
- 4.10 Liu, Y. Yan, Q. Tan, and G. Jin, “Theories for the design of diffractive superresolution elements and limits of optical superresolution,” *J. Opt. Soc. Am. A* **19**, 2185–2193 (2002)
- 4.11 Luo and C. Zhou, “Comparison of superresolution effects with annular phase and amplitude filters,” *Appl. Opt.* **34**, 6242-6247 (2004)
- 4.12 D. Li, and W. Zou, “Design and comparison of amplitude-type and phase-only transverse super-resolving pupil filters,” *Opt. Commun.* **229** 117–122, (2004)

Bibliography (Section 4 Continued)

- 4.13 H. Wang, and F. Gan, "New approach to superresolution," *Opt. Eng.* **40**, 851-855 (2001)
- 4.14 Wang, Z. Chen, and F. Gan, "High Focal Depth with a Pure-Phase Apodizer", *Appl. Opt.* **40**, 5658-5662 (2001)
- 4.15 Zhai, Y. Yann, D. Huang, M. Wu, and G. Jin, *Proc. SPIE* **3429**, 177 (1998)
- 4.16 M. de Juana, J. E. Oti, V. F. Canales, and M. P. Cagigal, "Design of superresolving continuous phase filters," *Opt. Lett.* **28**, 607-609 (2003)
- 4.17 Yun, L. Liu, J. Sun, and D. Liu, "Three-dimensional superresolution by three-zone complex pupil filters," *J. Opt. Soc. Am. A.* **22**, 272-277 (2005)
- 4.18 Y. Liu, and H. P. D. Shieh, "A novel dual focus objective lens for DVD/CD pick-up head," *IEEE TRANSACTIONS ON MAGNETICS*, **34**(1998)
- 4.19 G. Wilson, *Fourier Series and Optical Transform Techniques in Contemporary Optics*, (John Wiley & Sons, Inc.,1995)
- 4.20 Ledesma, J. Campos, J. C. Escalera, and M. J. Yzuel, "Simple expressions for performance parameters of complex filters, with applications to super-Gaussian phase filters", *Opt. Lett.* **29**, 932-934 (2004)

作者簡歷



本論文作者： 詹志雲 (Chih-Yun Chan)

台灣省嘉義縣人，民國71年生。

2000 畢業於協同中學。

2004 年取得清華大學電機工程學士學位。

2005 年於交通大學光電所取得碩士學位。

研究興趣為光學系統成像品質的分析與改善。

